nature ecology & evolution

Supplementary information

https://doi.org/10.1038/s41559-026-03044-y

Direct benefits are not necessary for the evolution of multicellularity

In the format provided by the authors and unedited

Contents

S1 Model for the evolution of multicellularity in a spatially heterogeneous environment

To explore the evolution of multicellularity, we model competition between a multicellular mutant and a unicellular ancestor. We introduce spatial heterogeneity by allowing cells to inhabit and migrate between two environments (A and B). We denote by y_A the density of ancestral single cells in environment A and by y_B the density of ancestral single cells in environment B. Moreover, $x_{n,A}$ and $x_{n,B}$ are the densities of mutant multicellular groups of size n in environments A and B, respectively. We define $\vec{x} \coloneqq (x_{1,A}, x_{2,A}, \ldots, x_{n,A}, x_{1,B}, x_{2,B}, \ldots, x_{n,B})$. Groups of the multicellular strategy grow and fragment according to their life cycle. We consider three types of life cycles:

N + 1: Once groups reach size $N+1$, they instantaneously split into a group of size N and a single-cell propagule.

N × 1: Once groups reach size N, they instantaneously disintegrate into N single-cell propagules.

N/2 + N/2: Once groups reach size N, they instantaneously split into two groups of equal size. If N is odd, one of the fragments ends up with an extra cell (i.e. one group with $(N+1)/2$ cells and another with $(N-1)/2$ cells).

Throughout this document, we will focus on the life cycles of the type $N+1$, but the expressions and results for the other life cycles can be found in the appendix.

S1.1 Model equations

Single cells of the unicellular life cycle divide at rate $r_{1,A}$ in environment A, and $r_{1,B}$ in environment B. The result of the division is two separate daughter cells. In this model, we do not consider density-independent mortality, so the division rates r can also be interpreted as per-capita intrinsic growth rates. Our results remain qualitatively unchanged when density-independent mortality is included (see Section S3). Cells migrate from environment A to environment B at rate $m_{1,AB}$ and from environment B to environment A at a possibly different rate $m_{1,BA}$. Individuals experience density-dependent mortality due to competition for the same resources. Groups die at rate $\gamma T_A(y,\vec{x})$ in environment A and at rate $\gamma T_B(y,\vec{x})$ in environment B, where, γ is a parameter that determines the strength of competition, and $T_A = y_A + \sum_{n\geq 1} n x_{n,A}$ and $T_B = y_B + \sum_{n\geq 1} n x_{n,B}$ are the total densities of cells in environments A and B, respectively. The density of ancestral cells in environment A changes according to

$$\frac{dy_A}{dt} = r_{1,A} y_A - \gamma T_A(y,\vec{x}) y_A - m_{1,AB} y_A + m_{1,BA} y_B, \tag{1}$$

while the density of ancestral cells in environment B follows

$$\frac{dy_B}{dt} = r_{1,B} y_B - \gamma T_B(y,\vec{x}) y_B - m_{1,BA} y_B + m_{1,AB} y_A. \tag{2}$$

Single cells of a multicellular life cycle divide, migrate, and die at the same rates as the single cells of the unicellular strategy. However, after division, these single cells stay together. Every subsequent division

leads to one more cell being added to the group until the fragmentation group size $(N+1)$ is reached. Cells in groups of size n divide at rate $r_{n,A}$ in environment A and at rate $r_{n,B}$ in environment B (where, again, density-independent death is not considered and the division rates are equal to the per capita growth rates). Groups of size n migrate from environment A to B at rate $m_{n,AB}$ and from environment B to A at rate $m_{n,BA}$. Finally, a group of size n in environment A dies from competition at a rate $\gamma T_A(y,\vec{x})$ and at rate $\gamma T_B(y,\vec{x})$ in environment B. The dynamics of the multicellular mutant population are given by

$$\frac{dx_{1,A}}{dt} = Nr_{N,A}x_{N,A} - r_{1,A}x_{1,A} - \gamma T_A(y,\vec{x})x_{1,A} - m_{1,AB}x_{1,A} + m_{1,BA}x_{1,B}, \tag{3}$$

$$\frac{dx_{1,B}}{dt} = Nr_{N,B}x_{N,B} - r_{1,B}x_{1,B} - \gamma T_B(y,\vec{x})x_{1,B} - m_{1,BA}x_{1,B} + m_{1,AB}x_{1,A} \tag{4}$$

for single cells,

$$\frac{dx_{i,A}}{dt} = (i-1)r_{i-1,A}x_{i-1,A} - ir_{i,A}x_{i,A} - \gamma T_A(y,\vec{x})x_{i,A} - m_{i,AB}x_{i,A} + m_{i,BA}x_{i,B}, \tag{5}$$

$$\frac{dx_{i,B}}{dt} = (i-1)r_{i-1,B}x_{i-1,B} - ir_{i,B}x_{i,B} - \gamma T_B(y,\vec{x})x_{i,B} - m_{i,BA}x_{i,B} + m_{i,AB}x_{i,A} \tag{6}$$

for groups of size $1 < i < N$, and

$$\frac{dx_{N,A}}{dt} = (N-1)r_{N-1,A}x_{N-1,A} - \gamma T_A(y,\vec{x})x_{N,A} - m_{N,AB}x_{N,A} + m_{N,BA}x_{N,B}, \tag{7}$$

$$\frac{dx_{N,B}}{dt} = (N-1)r_{N-1,B}x_{N-1,B} - \gamma T_B(y,\vec{x})x_{N,B} - m_{N,BA}x_{N,B} + m_{N,AB}x_{N,A} \tag{8}$$

for groups of size N. Note that the last equations do not contain negative terms $-Nr_{N,A}x_{N,A}$ and $-Nr_{N,B}x_{N,B}$ because groups of size N are not lost when they produce a single-celled propagule.

S2 Mathematical analysis of the model

S2.1 Dynamics of the unicellular ancestor

For multicellularity to evolve, a newly emerged multicellular mutant must be able to invade a population of the unicellular ancestor at steady state. Prior to the invasion, the two environments are exclusively occupied by single cells of the unicellular strategy, thus $T_A(y,\vec{x}) = y_A$ and $T_B(y,\vec{x}) = y_B$. The dynamics are given by (1) and (2). The resulting system

$$\begin{cases} \dfrac{dy_A}{dt} = r_{1,A}y_A - \gamma y_A^2 - m_{1,AB}y_A + m_{1,BA}y_B, \\ \dfrac{dy_B}{dt} = r_{1,B}y_B - \gamma y_B^2 - m_{1,BA}y_B + m_{1,AB}y_A. \end{cases} \tag{9}$$

always has the trivial steady state $(y_A, y_B) = (0,0)$. By carefully studying the phase diagram (Supplementary Figure 1), we can deduce that there is always a unique, stable steady state (y_A^*, y_B^*) with $y_A^*, y_B^* > 0$, while the trivial steady state $(0,0)$ is always unstable. There are three cases:

- When $r_{1,A} > m_{1,AB}$ and $r_{1,B} > m_{1,BA}$, we immediately see that the y_A- and y_B-nullclines (which are parabolas given by $m_{1,BA}y_B = y_A(\gamma y_A + m_{1,AB} - r_{1,A})$ and $m_{1,AB}y_A = y_B(\gamma y_B + m_{1,BA} - r_{1,B})$, respectively) intersect at a unique steady state (y_A^*, y_B^*) with y_A^*, $y_B^* > 0$; this is the case visualized in Supplementary Figure 1. We can also see from the phase diagram that $(0,0)$ is unstable and (y_A^*, y_B^*) is stable.
- When only one of $r_{1,A} > m_{1,AB}$ and $r_{1,B} > m_{1,BA}$ holds, $(0,0)$ becomes a saddle point. We can still draw the same conclusion directly from the phase diagram: the nullclines intersect at a unique, stable steady state (y_A^*, y_B^*) with y_A^*, $y_B^* > 0$, while $(0,0)$ remains unstable.
- When both $r_{1,A} < m_{1,AB}$ and $r_{1,B} < m_{1,BA}$, it is not immediately obvious from the phase diagram whether the nullclines intersect. However, they always do; this can be seen from comparing the slopes of the y_A- and y_B-nullclines at the origin. The slope of the y_A nullcline is $\left.\dfrac{\frac{dy_A}{dt}}{y_A}\right|_{y_A=0} = \dfrac{m_{1,AB} - r_{1,A}}{m_{1,BA}}$, while the y_B nullcline has a larger slope $\left(\left.\dfrac{\frac{dy_B}{dt}}{y_B}\right|_{y_B=0}\right)^{-1} = \dfrac{m_{1,AB}}{m_{1,BA} - r_{1,B}}$. Therefore, we can again conclude that there is a unique steady state (y_A^*, y_B^*) with y_A^*, $y_B^* > 0$. We confirm stability from the phase diagram.

Thus, the population of the unicellular ancestor always reaches a stable steady state.

Result S2.1: Steady state of the unicellular ancestor

The unicellular ancestor has a unique, stable steady state (y_A^*, y_B^*) with y_A^*, $y_B^* > 0$.

While it is not possible to obtain an analytical expression for (y_A^*, y_B^*), we can obtain an expression for the total cell density $y_A^* + y_B^*$ at this steady state. Indeed, from equations (1) and (2), we obtain the dynamics for

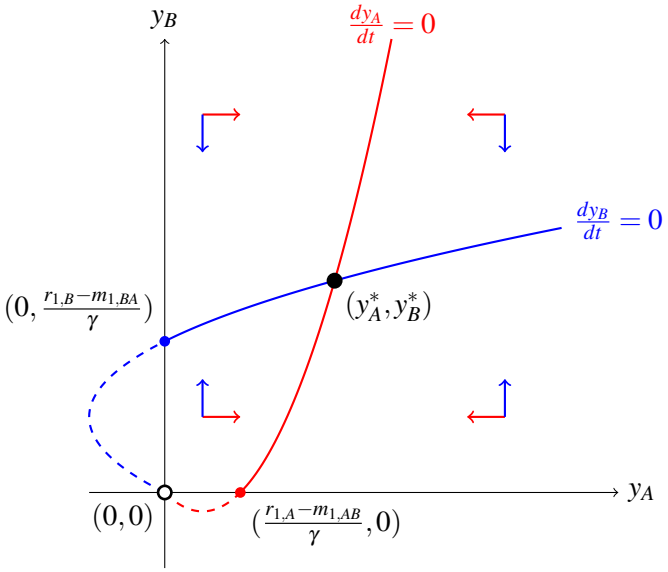

Supplementary Figure 1: Phase diagram for the dynamics of the unicellular ancestor. There is always a unique stable steady state (y_A^*, y_B^*) with $y_A^*, y_B^* > 0$.

$y_A + y_B$, given by

$$\frac{d}{dt}[y_A + y_B] = r_{1,A} y_A + r_{1,B} y_B - \gamma(y_A^2 + y_B^2). \tag{10}$$

At the non-trivial steady state, $y_A + y_B$ becomes

$$y_T = \frac{q_A r_{1,A} + q_B r_{1,B}}{\gamma(q_A^2 + q_B^2)}. \tag{11}$$

Here, $q_A = y_A/(y_A + y_B)$ is the fraction of ancestral cells that inhabit A at steady state; the remaining fraction $q_B = 1 - q_A$ inhabits environment B. Here, q_A and q_B are an emergent property of the ancestral population steady state and, in general, depend on the reproduction and migration parameters. Although we do not have an explicit expression for q_A and q_B—except for the fast migration limit, see section S2.5—these fractions can be obtained numerically by simulation equations (1) and (2) until they reach steady state.

S2.2 Dynamics of the multicellular mutant during invasion from rare

At the initial stages of invasion, the unicellular ancestor is at steady state ($y_A = q_A y_T$ and $y_B = q_B y_T$) and the multicellular mutant population is very small ($x_{n,A} \approx x_{n,B} \ll y_A, y_B$, for all n). Consequently, the total density of cells in both environments is $T_A(y, \vec{x}) \approx q_A y_T$ and $T_B(y, \vec{x}) \approx q_B y_T$. Therefore, equations (3)-(8) become linear at this initial stage of invasion.

In this linear regime, the dynamics of the multicellular mutant population are dictated by the Jacobian matrix $\mathbf{M}$ associated with equations (3)-(8). That is,

$$\frac{d}{dt}\vec{x} = \mathbf{M}\,\vec{x}, \tag{12}$$

As long as the dynamics between environments A and B are coupled (i.e., $\sum_{i=1}^{N} m_{i,AB} > 0$ and $\sum_{i=1}^{N} m_{i,BA} > 0$), the linearity of (12) ensures that $\vec{x}$ eventually aligns with the dominant eigenvector

$$\vec{v} = (v_{1,A},\, v_{2,A}, \ldots,\, v_{n,A},\, v_{1,B},\, v_{2,B}, \ldots,\, v_{n,B}), \tag{13}$$

in such a way that

$$\vec{x}(t) \approx X_0 e^{\lambda t} \vec{v}, \tag{14}$$

with X_0 being an arbitrary constant associated with the initial conditions and λ the dominant eigenvalue. That is, during the invasion from rare, the population growth rate becomes the dominant eigenvalue λ and the population structure (the relative values of $x_{n,A}$ and $x_{n,B}$ with respect to each other) becomes constant and given by the dominant eigenvector $\vec{v}$ [2]. This means that the fraction of groups of size n in environment A is also constant and given by

$$p_{n,A} = \frac{x_{n,A}}{x_{n,A} + x_{n,B}} = \frac{X_0 e^{\lambda t} v_{n,A}}{X_0 e^{\lambda t} v_{n,A} + X_0 e^{\lambda t} v_{n,B}} = \frac{v_{n,A}}{v_{n,A} + v_{n,B}}. \tag{15}$$

Analogously, the fraction of groups of size n in environment B is also constant and given by $p_{n,B} = 1 - p_{n,A}$. Importantly, we cannot find the general expressions of $p_{n,A}$ and $p_{n,B}$ in terms of our parameters, but knowing that the spatial distribution stabilizes (i.e., $p_{n,A}$ and $p_{n,B}$ are constant) during the initial stages of the invasion suffices for the rest of our analysis.

Because the spatial distribution of groups is constant during the invasion from rare, the only dynamical variables here are the densities of groups $x_n = x_{n,A} + x_{n,B}$, for $1 \leq n \leq N$. We can write the dynamical equations for x_n from equations (3)-(8) by using the relations $x_{n,A} = p_{n,A} x_n$ and $x_{n,B} = p_{n,B} x_n$. To simplify our equations, we define

$$\bar{r}_n = p_{n,A}\, r_{n,A} + p_{n,B}\, r_{n,B} \tag{16}$$

as the average growth rate of cells in groups of size n and

$$\bar{c}_n = \gamma y_T (p_{n,A}\, q_A + p_{n,B}\, q_B) \tag{17}$$

as the average death rate (from competition) of cells in groups of size n. Then, in (3)-(8), by adding each $\frac{dx_{n,A}}{dt}$ with the corresponding $\frac{dx_{n,B}}{dt}$, we obtain the dynamics of the multicellular mutant population as

$$\frac{dx_1}{dt} = N \bar{r}_N x_N - (\bar{r}_1 + \bar{c}_1) x_1, \tag{18}$$

$$\frac{dx_i}{dt} = (i-1) \bar{r}_{i-1} x_{i-1} - (i \bar{r}_i + \bar{c}_i) x_i, \tag{19}$$

$$\frac{dx_N}{dt} = (N-1) \bar{r}_{N-1} x_{N-1} - \bar{c}_N x_N, \tag{20}$$

with $1 < i < N$.

Result S2.2: Mutant dynamics during invasion

During the initial invasion from rare, the dynamics of a multicellular mutant with life cycle $N+1$ are given by

$$\begin{cases} \dfrac{dx_1}{dt} &= N\bar{r}_N x_N - (\bar{r}_1+\bar{c}_1)x_1, \\ \dfrac{dx_i}{dt} &= (i-1)\bar{r}_{i-1}x_{i-1} - (i\bar{r}_i+\bar{c}_i)x_i, \qquad \text{(where } 1<i<n\text{)} \\ \dfrac{dx_N}{dt} &= (N-1)\bar{r}_{N-1}x_{N-1} - \bar{c}_N x_N, \end{cases}$$

where $\bar{r}_n$ and $\bar{c}_n$ are given by (16) and (17).

S2.3 Condition for the invasion of the multicellular mutant

For a successful invasion to occur, the mutant population must be able to grow when rare. As established in (14), the mutant population $\vec{x}$ aligns with the dominant eigenvector $\vec{v}$, and all x_n change exponentially with the same exponent λ, the dominant eigenvalue. A successful invasion represents the scenario where $\lambda > 0$, and thus $dx_n/dt \propto \lambda > 0$ for $1 \le n \le N$. From Result S2.2, the $dx_n/dt > 0$ condition leads to

$$x_1 < \frac{N\bar{r}_N}{\bar{r}_1+\bar{c}_1}x_N, \qquad x_i < \frac{(i-1)\bar{r}_{(i-1)}}{i\bar{r}_i+\bar{c}_i}x_{i-1}, \qquad \text{and} \qquad x_N < \frac{(N-1)\bar{r}_{(N-1)}}{\bar{c}_N}x_{N-1}, \tag{21}$$

with $1 < i < N$. The first condition above can be combined with the second (for $i = 2$), giving us

$$x_2 < \frac{\bar{r}_1}{2\bar{r}_2+\bar{c}_2}\frac{N\bar{r}_N}{\bar{r}_1+\bar{c}_1}x_N. \tag{22}$$

Incorporating the conditions obtained from the other $dx_n/dt > 0$ inequalities, we get

$$x_N < x_N\left[\frac{N\bar{r}_N}{\bar{c}_N}\prod_{i=1}^{N-1}\frac{i\bar{r}_i}{i\bar{r}_i+\bar{c}_i}\right]. \tag{23}$$

Thus, a necessary (and, as we will see later, also sufficient) condition for the the multicellular mutant to be able to invade is

$$\rho(N) = \frac{N\bar{r}_N}{\bar{c}_N}\prod_{n=1}^{N-1}\frac{n\bar{r}_n}{n\bar{r}_n+\bar{c}_n} > 1. \tag{24}$$

We can interpret $\rho(N)$ as the basic reproduction number of a $N+1$ life cycle: it is the expected number of single cell propagules generated by a group across its lifespan, which is the probability that a single cell will grow into a group of size N (i.e. $\prod_{n=1}^{N-1}\frac{n\bar{r}_n}{n\bar{r}_n+\bar{c}_n}$) times the expected number of propagules generated at the "N" stage (i.e. $\frac{N\bar{r}_N}{\bar{c}_N}$). Then, multicellularity can only invade if a group undergoing a $N+1$ life cycle is expected to generate more than one propagule before it dies, i.e. $\rho(N) > 1$.

We perform a similar analysis on the other two possible scenarios where multicellularity does not invade. When the mutant population decreases (i.e., $dx_n/dt \propto \lambda < 0$, for $1 \le n \le N$), we find that $\rho(N) < 1$ must hold. If the mutant population stays constant (i.e., $dx_n/dt = \lambda = 0$, for $1 \le n \le N$), we get $\rho(N) = 1$. Thus,

the reproduction number $\rho(N)$ determines whether a multicellular mutant of the $N+1$ life cycle invades ($\rho(N) > 1$), goes extinct ($\rho(N) < 1$), or persists neutrally at a low frequency ($\rho(N) = 1$).

Result S2.3: Invasion condition

The immediate fate of a multicellular mutant with a $N+1$ life cycle is determined by its reproduction number

$$\rho(N) = \frac{N\bar{r}_N}{\bar{c}_N} \prod_{n=1}^{N-1} \frac{n\bar{r}_n}{n\bar{r}_n + \bar{c}_n}.$$

The mutant successfully invades when $\rho(N) > 1$, persists neutrally when $\rho(N) = 1$, and goes extinct when $\rho(N) < 1$.

Result S2.3 reveals that the outcome of the invasion is determined by the relative magnitudes of reproduction ($\bar{r}_n$ with $1 \leq n \leq N$) and death by competition ($\bar{c}_n$ with $1 \leq n \leq N$). In fact, the ratio between these quantities—$\bar{r}_n$ and $\bar{c}_n$—can be thought of as the reproduction number of a cell in a group of size n:

$$\rho_{\text{cell}}(n) = \frac{\bar{r}_n}{\bar{c}_n} = \frac{p_{n,A}\, r_{n,A} + p_{n,B}\, r_{n,B}}{\gamma(p_{i,A}\, q_A + p_{i,B}\, q_B) y_T}, \tag{25}$$

that is, reproduction rate ($\bar{r}_n$) times expected life span ($1/\bar{c}_n$). Recalling expression (11) for y_T, we get

$$\rho_{\text{cell}}(n) = \frac{p_{n,A}\, r_{n,A} + p_{n,B}\, r_{n,B}}{q_A r_{1,A} + q_B r_{1,B}} \cdot \frac{q_A^2 + q_B^2}{p_{n,A}\, q_A + p_{n,B}\, q_B} = \frac{R_n}{C_n}, \tag{26}$$

where

$$R_n := \frac{p_{n,A}\, r_{n,A} + p_{n,B}\, r_{n,B}}{q_A r_{1,A} + q_B r_{1,B}} \tag{27}$$

is the average growth rate of cells in groups of size n, relative to the average growth rate of the ancestor, and

$$C_n := \frac{p_{n,A}\, q_A + p_{n,B}\, q_B}{q_A^2 + q_B^2} \tag{28}$$

is the average competition from ancestral cells experienced by cells in groups of size n, relative to the average competition experienced by the ancestor. Expression (24) can be reorganized in order to be expressed exclusively in terms of R_n/C_n,

$$\rho(N) = N! \frac{R_N}{C_N} \prod_{n=1}^{N-1} \frac{1}{n + \frac{C_n}{R_n}}. \tag{29}$$

We conclude that the fate of the mutant is completely determined by the ratios R_n/C_n.

Result S2.4: Equivalent invasion condition

A necessary and sufficient condition for the invasion of a multicellular mutant with an $N+1$ life cycle is

$$N! \frac{R_N}{C_N} \prod_{n=1}^{N-1} \frac{1}{n + \frac{C_n}{R_n}} > 1.$$

S2.4 Consequences of the invasion condition

Result S2.4 has a number of key consequences. The first is a necessary (but not sufficient) condition for invasion to succeed.

Result S2.5: A necessary condition for invasion to be successful

Multicellularity can only invade if $R_n/C_n > 1$ for at least one group size n.

Indeed, if $R_n/C_n \leq 1$ for all $1 \leq n \leq N$, then we would find

$$N! \frac{R_N}{C_N} \prod_{n=1}^{N-1} \frac{1}{n + \frac{C_n}{R_n}} \leq N! \prod_{n=1}^{N-1} \frac{1}{n+1} = 1, \tag{30}$$

which according to Result S2.4 means that the multicellular mutant would *not* be able to invade.

Moreover, in the special case that there is only one environment (say, A), we have $q_A = 1$, $q_B = 0$, and also $p_{n,A} = 1$, $p_{n,B} = 0$ for every group size n. Equations (27) and (28) simplify to

$$R_n = \frac{r_{n,A}}{r_{1,A}} \qquad \text{and} \qquad C_n = 1, \tag{31}$$

so the condition $R_n/C_n > 1$ for at least some n becomes that $r_{n,A} > r_{1,A}$ for at least some n. Thus, in a single environment, multicellularity can only invade if at least some group size n provides a direct benefit.

Result S2.6: Invasion condition when there is no spatial heterogeneity

In the absence of spatial heterogeneity, multicellularity requires direct benefits to evolve: multicellularity can only invade if $r_{n,A} > r_{n,1}$ for at least one n.

Finally, we consider what happens in the special case that $N = 2$. According to Result S2.4, a necessary and sufficient for a $2+1$ mutant to be able to invade is

$$2 \cdot \frac{R_2}{C_2} \cdot \frac{1}{1 + \frac{C_1}{R_1}} > 1 \iff \frac{R_1}{C_1} \left(2 \cdot \frac{R_2}{C_2} - 1 \right) > 1. \tag{32}$$

However, Figure 2 in the main text suggests that multicellularity can only invade if $R_1/C_1 > 1$: there are no points in the shaded region for which $R_1/C_1 < 1$. In fact, something even stronger is true for the $2+1$ life cycle: if $R_1/C_1 < 1$, then we must have $R_2/C_2 < R_1/C_1$. In this section, we give a formal proof of this statement.

Result S2.7: Conditions for the $2+1$ life cycle

For the $2+1$ life cycle in the absence of indirect benefits, $\frac{R_1}{C_1} < 1$ implies $\frac{R_2}{C_2} < \frac{R_1}{C_1}$. In particular, multicellularity cannot invade if $\frac{R_1}{C_1} < 1$.

The proof is by contradiction: we show that it is impossible that $R_1/C_1 < 1$ and $R_1/C_1 < R_2/C_2$ hold simultaneously. We first observe that $R_1/C_1 < 1$ implies that

$$(p_{1,A}r_{1,A} + p_{1,B}r_{1,B})(q_A^2 + q_B^2) < (q_A r_{1,A} + q_B r_{1,B})(q_A p_{1,A} + q_B p_{1,B}), \tag{33}$$

which can be rearranged to

$$\left(\frac{q_A}{q_B} - \frac{r_{1,A}}{r_{1,B}}\right)\left(\frac{p_{1,A}}{p_{1,B}} - \frac{q_A}{q_B}\right) > 0. \tag{34}$$

On the other hand, $R_1/C_1 < R_2/C_2$ tells us that

$$\frac{q_A p_{2,A} + q_B p_{2,B}}{q_A p_{1,A} + q_B p_{1,B}} < \frac{p_{2,A}r_{2,A} + p_{2,B}r_{2,B}}{p_{1,A}r_{1,A} + p_{1,B}r_{1,B}} < \frac{p_{2,A}r_{1,A} + p_{2,B}r_{1,B}}{p_{1,A}r_{1,A} + p_{1,B}r_{1,B}}, \tag{35}$$

where we have used $r_{2,A} < r_{1,A}$ and $r_{2,B} < r_{1,B}$ (i.e., no direct benefits) for the last step. We can rearrange (35) to

$$\left(\frac{p_{1,A}}{p_{1,B}} - \frac{p_{2,A}}{p_{2,B}}\right)\left(\frac{q_A}{q_B} - \frac{r_{1,A}}{r_{1,B}}\right) > 0. \tag{36}$$

Multiplying (34) and (36) and dividing by $\left(\frac{q_A}{q_B} - \frac{r_{1,A}}{r_{1,B}}\right)^2 > 0$ yields

$$\left(\frac{p_{1,A}}{p_{1,B}} - \frac{p_{2,A}}{p_{2,B}}\right)\left(\frac{p_{1,A}}{p_{1,B}} - \frac{q_A}{q_B}\right) > 0, \tag{37}$$

which tells us that

$$\frac{p_{1,A}}{p_{1,B}} > \max\left(\frac{p_{2,A}}{p_{2,B}}, \frac{q_A}{q_B}\right) \qquad \text{or} \qquad \frac{p_{1,A}}{p_{1,B}} < \min\left(\frac{p_{2,A}}{p_{2,B}}, \frac{q_A}{q_B}\right). \tag{38}$$

But this is impossible, because the spatial distribution of the 1-cell stage of the $2+1$ life cycle is always "in between" the spatial distributions of the unicellular ancestor and the 2-cell stage of the $2+1$ life cycle.

S2.5 Model simplification in the limit of fast migration

We consider the special case in which the migration dynamics are much faster than the birth-death dynamics, i.e., limit of $m_{n,AB}, m_{n,BA} \to \infty$. This creates a separation of timescales between reproduction and migration, allowing for the migration dynamics to reach steady state instantaneously. This means that

$$\frac{y_A}{y_A + y_B}, \frac{x_{1,A}}{x_{1,A} + x_{1,B}} \quad \text{equilibrate at} \quad \frac{m_{1,BA}}{m_{1,AB} + m_{1,BA}} := p_{1,A} = q_A, \tag{39}$$

$$\frac{x_{n,A}}{x_{n,A} + x_{n,B}} \quad \text{equilibrates at} \quad \frac{m_{n,BA}}{m_{n,AB} + m_{n,BA}} := p_{n,A}. \tag{40}$$

Similarly,

$$\frac{y_B}{y_A + y_B}, \frac{x_{1,B}}{x_{1,A} + x_{1,B}} \quad \text{equilibrate at} \quad \frac{m_{1,AB}}{m_{1,AB} + m_{1,BA}} := p_{1,B} = q_B, \tag{41}$$

$$\frac{x_{n,B}}{x_{n,A} + x_{n,B}} \quad \text{equilibrates at} \quad \frac{m_{n,AB}}{m_{n,AB} + m_{n,BA}} := p_{n,B}. \tag{42}$$

Therefore, under these assumptions of fast migration, the dynamics simplify substantially: the spatial distribution of the populations over the two environments (q_A, q_B, $p_{n,A}$, and $p_{n,B}$) is completely determined by the migration rates. In addition, single cells from multicellular and unicellular strategies have the same spatial distribution ($p_{1,A} = q_A$ and $p_{1,B} = q_B$). With a fixed spatial distribution, the dynamics of this system are fully determined by the total population of ancestral cells ($y_T = y_A + y_B$) and the total populations of groups of different sizes n ($x_n = x_{n,A} + x_{n,B}$). Then, from (1)-(8), we get

$$\frac{dy_T}{dt} = (\bar{r}_1 - \bar{c}_1(y_T, \vec{x}))\, y_T, \tag{43}$$

$$\frac{dx_1}{dt} = N\bar{r}_N x_N - (\bar{r}_1 + \bar{c}_1(y_T, \vec{x}))\, x_1, \tag{44}$$

$$\frac{dx_i}{dt} = (i-1)\bar{r}_{i-1}x_{i-1} - (i\bar{r}_i + \bar{c}_i(y_T, \vec{x}))\, x_i, \tag{45}$$

$$\frac{dx_N}{dt} = (N-1)\bar{r}_{N-1}x_{N-1} - \bar{c}_N(y_T, \vec{x})x_N, \tag{46}$$

with $1 < i < N$. Again, $\bar{r}_n = p_{n,A}\, r_{n,A} + p_{n,B}\, r_{n,B}$ is the average growth rate of cells in groups of size n and $\bar{c}_n(y_T, \vec{x}) = \gamma(p_{n,A}T_A(y_T, \vec{x}) + p_{n,B}T_B(y_T, \vec{x}))$ is the average death rate—from competition—of cells in groups of size n. Also, the total density of cells in environment A simplifies to $T_A(y_T, \vec{x}) = p_{1,A}y_T + \sum_{n=1}^{N} np_{n,A}x_n$, and $T_B(y_T, \vec{x}) = p_{1,B}y_T + \sum_{n=1}^{N} np_{n,B}x_n$ for environment B.

S2.6 Model extension with density-independent mortality of groups

Here, we add a term accounting for density-independent mortality in (1)–(8), due to, e.g., senescence. We assume that groups of size n die at rate $d_{n,A}$ in environment A and $d_{n,B}$ in environment B. When a group dies, all its member cells simultaneously die as well. Thus, the per capita density-independent death rate for a group of size n—and, consequently, for any of its constituent cells—is $d_{n,A}$ or $d_{n,B}$, depending on the environment. Then, the per capita growth rate is

$$r_{n,A} = b_{n,A} - d_{n,A} \tag{47}$$

in environment A and

$$r_{n,B} = b_{n,B} - d_{n,B} \tag{48}$$

in environment B. The system's equations (1)-(8) then become

$$\frac{dy_A}{dt} = r_{1,A}y_A - \gamma T_A(y, \vec{x})y_A - m_{1,AB}y_A + m_{1,BA}y_B, \tag{49}$$

$$\frac{dy_B}{dt} = r_{1,B}y_B - \gamma T_B(y, \vec{x})y_B - m_{1,BA}y_B + m_{1,AB}y_A, \tag{50}$$

for the unicellular ancestor, and

$$\frac{dx_{1,A}}{dt} = Nb_{N,A}x_{N,A} - (b_{1,A}+d_{1,A})x_{1,A} - \gamma T_A(y,\vec{x})x_{1,A} - m_{1,AB}x_{1,A} + m_{1,BA}x_{1,B}, \tag{51}$$

$$\frac{dx_{1,B}}{dt} = Nb_{N,B}x_{N,B} - (b_{1,B}+d_{1,B})x_{1,B} - \gamma T_B(y,\vec{x})x_{1,B} - m_{1,BA}x_{1,B} + m_{1,AB}x_{1,A}, \tag{52}$$

$$\frac{dx_{i,A}}{dt} = (i-1)b_{i-1,A}x_{i-1,A} - i(b_{i,A}+d_{i,A})x_{i,A} - \gamma T_A(y,\vec{x})x_{i,A} - m_{i,AB}x_{i,A} + m_{i,BA}x_{i,B}, \tag{53}$$

$$\frac{dx_{i,B}}{dt} = (i-1)b_{i-1,B}x_{i-1,B} - i(b_{i,B}+d_{i,B})x_{i,B} - \gamma T_B(y,\vec{x})x_{i,B} - m_{i,BA}x_{i,B} + m_{i,AB}x_{i,A}, \tag{54}$$

$$\frac{dx_{N,A}}{dt} = (N-1)b_{N-1,A}x_{N-1,A} - d_{N,A}x_{N,A} - \gamma T_A(y,\vec{x})x_{N,A} - m_{N,AB}x_{N,A} + m_{N,BA}x_{N,B}, \tag{55}$$

$$\frac{dx_{N,B}}{dt} = (N-1)b_{N-1,B}x_{N-1,B} - d_{N,B}x_{N,B} - \gamma T_B(y,\vec{x})x_{N,B} - m_{N,BA}x_{N,B} + m_{N,AB}x_{N,A} \tag{56}$$

for the $N+1$ multicellular mutant, with $1 < i < N$. Therefore, in this model, groups die both from senescence, at a density-independent rate determined by the d parameters, and competition, at a density-dependent rate determined by γT_A and γT_B.

Performing an invasion analysis (analogous to Section S2), we obtain the reproduction number for the system of equations (51)-(56), given by

$$\rho(N) = \frac{N\bar{b}_N}{\bar{d}_N + \bar{c}_N} \prod_{n=1}^{N-1} \frac{n\bar{b}_n}{n\bar{b}_n + \bar{d}_n + \bar{c}_n}, \tag{57}$$

where $\bar{b}_n = p_{n,A}b_{n,A} + p_{n,B}b_{n,B}$ is the average division rate and $\bar{d}_n = p_{n,A}d_{n,A} + p_{n,B}d_{n,B}$ is the average death rate of a cell in a group of size $n > 0$. $\bar{c}_n = \gamma y_T(p_{n,A}\, q_A + p_{n,B}\, q_B)$ is the average death by competition experienced by a cell in a group of size n. As the expression for the stationary density of ancestral cells before invasion y_T remains unchanged from (11), $\bar{c}_n$ is

$$\bar{c}_n = \gamma \cdot (p_{n,A}\, q_A + p_{n,B}\, q_B)\frac{q_A r_{1,A} + q_B r_{1,B}}{\gamma \cdot (q_A^2 + q_B^2)} = (q_A r_{1,A} + q_B r_{1,B}) \cdot C_n. \tag{58}$$

where C_n is the average competition experienced by a cell in a group of size n relative to the competition experienced by the unicellular ancestor, as in (28). The expression of the reproduction number (57) can be reorganized to become

$$\rho(N) = \left[1 + \frac{\bar{r}_N}{\bar{b}_N}\left(\frac{C_N}{R_N} - 1\right)\right]^{-1} \prod_{n}^{N-1} \left[1 + \frac{\bar{r}_n}{(n+1)\bar{b}_n}\left(\frac{C_n}{R_n} - 1\right)\right]^{-1}. \tag{59}$$

$\bar{r}_n = p_{n,A}\, r_{n,A} + p_{n,B}\, r_{n,B} = p_{n,A}\, (b_{n,A} - d_{n,A}) + p_{n,B}\, (b_{n,B} - d_{n,B})$ is the average growth rate of a cell in a group of size n. Likewise,

$$R_n = \frac{p_{n,A}\, r_{n,A} + p_{n,B}\, r_{n,B}}{q_A\, r_{1,A} + q_B\, r_{1,B}} = \frac{p_{n,A}\, (b_{n,A} - d_{n,A}) + p_{n,B}\, (b_{n,B} - d_{n,B})}{q_A\, (b_{1,A} - d_{1,A}) + q_B\, (b_{1,B} - d_{1,B})} \tag{60}$$

is the average growth rate of a cell in a group of size n relative to the ancestral cells, as in (27).

Result S2.8: Invasion condition for a more general model that includes group death

For a more general that decomposes net growth rates r_n as the difference between cell division rates b_n and group death rates d_n, the reproduction number of a multicellular mutant with an $N+1$ life cycle is

$$\rho(N) = \left[1 + \frac{\bar{r}_N}{\bar{b}_N}\left(\frac{C_N}{R_N} - 1\right)\right]^{-1} \prod_n^{N-1} \left[1 + \frac{\bar{r}_n}{(n+1)\bar{b}_n}\left(\frac{C_n}{R_n} - 1\right)\right]^{-1},$$

where R_n is now given by (60). The mutant invades if and only if $\rho(N) > 1$.

Note that if $d_n = 0$ for all $n > 0$, then $\bar{r}_n = \bar{b}_n$, and the expression for the reproduction number in (59) becomes equivalent to that of the previous model (29). Thus, the main difference introduced by including density-independent death is a weighting factor proportional to $\bar{r}_n/\bar{b}_n$, which adjusts the contribution of each term R_n/C_n. Also, as in the model without density-independent death (Eq. (1)-(8)), multicellularity can invade only if $R_n/C_n > 1$ for at least one group size n. That is, multicellularity can evolve only if at least one stage $n \geq 1$ of the life cycle obtains indirect benefits through escape of competition ($C_n < 1$), environmental exploitation ($R_n > 1$), or both. Therefore, the condition for the invasion of a multicellular life cycle remains qualitatively unchanged when density-independent death is included.

S3 A case study: incipient multicellularity in the Proterozoic Ocean

In this section we present our model for the evolution of multicellularity in the Proterozoic Ocean and the associated simulation results.

S3.1 Generalization of the model to multiple multicellular life cycles

We present an extended version of the model in which multiple multicellular life cycles can be simultaneously present. We use this extended version to simulate the evolutionary dynamics that arise when mutant multicellular life cycles with different fragmentation sizes repeatedly attempt to invade.

We build this model under the fast-migration limit, where we only need to keep track of the total populations of the ancestral cells ($y = y_A + y_B$) and the total population of groups ($x_n = x_{n,A} + x_{n,B}$). Then, the dynamics are analogous to (43)-(46), with the exception that multiple $N+1$ life cycles (with different fragmentation sizes) can exist simultaneously. We introduce the upper index N to x_n^N to specify the life cycle $N+1$ that a given group of size n belongs to (e.g., x_3^5 counts groups of size 3 belonging to a $5+1$ life cycle). Under this representation, the population size of cells of a unicellular strategy can be expressed as $x_1^1 := y$—i.e., groups of size 1 of a $1+1$ life cycle. We also re-define $\vec{x}$ to encompass all life cycles present: $\vec{x} := (x_1^1, x_1^2, x_2^2, \ldots, x_n^N, x_{n+1}^N, \ldots)$. Then, the system of differential equations that describe the dynamics of a population undergoing a $N+1$ life cycle is

$$\frac{dx_1^1}{dt} = (\bar{r}_1 - \bar{c}_1(\vec{x}))\, x_1^1, \tag{61}$$

for $N = 1$, and

$$\frac{dx_1^N}{dt} = N\bar{r}_N x_N^N - (\bar{r}_1 + \bar{c}_1(\vec{x}))\, x_1^N, \tag{62}$$

$$\frac{dx_i^N}{dt} = (i-1)\bar{r}_{i-1} x_{i-1}^N - (i\bar{r}_i + \bar{c}_i(\vec{x}))\, x_i^N, \tag{63}$$

$$\frac{dx_N^N}{dt} = (N-1)\bar{r}_{N-1} x_{N-1}^N - \bar{c}_N(\vec{x}) x_N^N, \tag{64}$$

for all $N > 1$. Here, the total density of cells in an environment A accounts for every group from every life cycle present, i.e., $T_A(\vec{x}) := \sum_{N\geq 1}\sum_{n=1}^N n p_{n,A} x_n^N$. Similarly, for environment B, $T_B(\vec{x}) := \sum_{N\geq 1}\sum_{n=1}^N n p_{n,B} x_n^N$. Then, the average death rate—from competition—of cells in groups of size n is $\bar{c}_n(\vec{x}) = \gamma(p_{n,A}T_A(\vec{x}) + p_{n,B}T_B(\vec{x}))$. Finally, the average growth rate of cells in groups of size n is $\bar{r}_n = p_{n,A}r_{n,A} + p_{n,B}r_{n,B}$.

S3.2 Generalized invasion conditions

The dynamics will eventually reach a steady state community, represented by

$$\vec{u} := (u_1^1, u_1^2, u_2^2, \ldots, u_n^N, u_{n+1}^N, \ldots), \tag{65}$$

such that $d\vec{u}/dt = 0$ (we never observe oscillatory behavior). Imagine that the $1+1$ life cycle is part of this steady state community. Then,

$$\frac{du_1^1}{dt} = (\bar{r}_1 - \bar{c}_1^*)u_1^1 = 0, \tag{66}$$

with $\bar{c}_n(\vec{u}) := \bar{c}_n^*$. The equation above has a non-trivial solution (i.e., $u_1^1 \neq 0$) when the basic reproduction number of the $1+1$ life cycle equals one, i.e., $\rho(1) := \bar{r}_1/\bar{c}_1^* = 1$. Analogously, imagine an arbitrary life cycle $N+1$ is present at the steady state community. Then, from (62)-(64), $du_n^N/dt = 0$ for $1 \leq n \leq N$ implies

$$u_1^N = \frac{N\bar{r}_N}{\bar{r}_1 + \bar{c}_1^*} u_N^N, \qquad u_i^N = \frac{(i-1)\bar{r}_{(i-1)}}{i\bar{r}_i + \bar{c}_i^*} u_{i-1}^N, \qquad \text{and} \qquad u_N^N = \frac{(N-1)\bar{r}_{(N-1)}}{\bar{c}_N^*} u_{N-1}^N, \tag{67}$$

with $1 < i < N$. If we combine the equations above, we obtain

$$u_N^N = u_N^N \left[\frac{N\bar{r}_N}{\bar{c}_n^*} \prod_{i=1}^{n-1} \frac{i\bar{r}_i}{i\bar{r}_i + \bar{c}_i^*} \right] \tag{68}$$

where

$$\rho(N) = \frac{N\bar{r}_N}{\bar{c}_N^*} \prod_{n=1}^{N-1} \frac{n\bar{r}_n}{n\bar{r}_n + \bar{c}_n^*} \tag{69}$$

is the basic reproduction number of the $N+1$ life cycle, with $N > 1$. Thus, the reproduction number of any life cycle present at steady state must equal one, that is, $\rho(N) = 1$.

Now, imagine that a rare $M+1$ mutant population attempts to invade this steady state community. As in Result S2.3, the reproduction number (69) determines whether such a multicellular mutant invades ($\rho(M) > 1$), goes extinct ($\rho(M) < 1$), or persists neutrally at a low frequency ($\rho(M) = 1$).

S3.3 The Proterozoic Ocean model

We work in the fast-migration limit and assume that a proportion $1 \geq q_A \geq 0.5$ of single cells inhabit the upper layer of the water column (environment A) while a proportion $q_B = 1 - q_A$ inhabit the lower layer of the water column (environment B). Groups below a critical size N_S are also buoyant and have the same distribution (q_A and q_B) as single cells. Once the critical size is reached, groups instantly sink to a lower layer (environment B) that is more oxygen-deprived. In the main text, we set $q_B = 0$; we explore the effects of mixing ($q_B > 0$) in Section S3.6.

The spatial distribution of groups of any given size n is

$$p_{n,A} = \begin{cases} q_A & \text{if } n < N_S; \\ 0 & \text{if } n \geq N_S, \end{cases} \qquad \text{and} \qquad p_{n,B} = \begin{cases} q_B & \text{if } n < N_S; \\ 1 & \text{if } n \geq N_S. \end{cases} \tag{70}$$

The average death rates by competition for a cell in a group of size n is

$$\bar{c}_i(\vec{x}) = \begin{cases} \gamma T_A(\vec{x}) & \text{if } i < N_S, \\ \gamma T_B(\vec{x}) & \text{if } i \geq N_S, \end{cases} \tag{71}$$

where $T_A = \sum_{N \geq 1} \sum_{n=1}^{N_S - 1} q_A n x_n^N$ and $T_B = \sum_{N \geq 1} \left[\sum_{n=1}^{N_S - 1} q_B n x_n^N + \sum_{n=N_S}^{N} n x_n^N \right]$.

In the upper layer of the water column, cells in small multicellular groups perform respiration and divide at high rates (r_o); after a critical group size N_U, we assume that oxygen cannot diffuse deeper into the

multicellular body, and any cells past the critical size are limited to doing fermentation with a lower division rate r_f. Thus, the growth rates in the upper layer are given by

$$r_{n,A} = \begin{cases} r_o & \text{if } n \leq N_U; \\ \dfrac{N_U \cdot r_o + (n - N_U) \cdot r_f}{n} & \text{if } n > N_U. \end{cases} \tag{72}$$

In the more oxygen-deprived lower layer, diffusion limitation occurs at a smaller group size in such a way that the maximal number of respiring cells in each group is reduced from N_U to $N_L \leq N_U$. When $N_L = 0$, the lower layer is completely deprived of oxygen, and all cells in it are limited to fermentation, i.e. $r_{n,B} = r_f$ for every n. Furthermore, $N_U = 0$ corresponds to an anoxic world where all cells are limited to fermentation, i.e., $r_{n,A} = r_{n,B} = r_f$ for every n. In a general scenario, the growth rates in the lower layer are

$$r_{n,B} = \begin{cases} r_o & \text{if } 0 < n \leq N_L; \\ \dfrac{N_L \cdot r_o + (n - N_L) \cdot r_f}{n} & \text{if } n > N_L. \end{cases} \tag{73}$$

The average growth rate of cells in groups of size $n < N_S$ is $\bar{r}_{n,A} = q_A r_{n,A} + q_B r_{n,B}$, with $\bar{r}_{n,A} = r_{n,A}$ when spatial separation is perfect ($q_B = 0$).

For these specific choices of spatial distribution and migration rates, the model's equations (61)-(64) become

$$\frac{dx_1^1}{dt} = (\bar{r}_{1,A} - \gamma T_A(\vec{x}))\, x_1^1, \tag{74}$$

for $N = 1$,

$$\frac{dx_1^N}{dt} = N\bar{r}_{N,A} x_N^N - (\bar{r}_{1,A} + T_A(\vec{x}))\, x_1^N, \tag{75}$$

$$\frac{dx_i^N}{dt} = (i-1)\bar{r}_{i-1,A} x_{i-1}^N - (i\bar{r}_{i,A} + T_A(\vec{x}))\, x_i^N, \tag{76}$$

$$\frac{dx_N^N}{dt} = (N-1)\bar{r}_{N-1,A} x_{N-1}^N - T_A(\vec{x}) x_N^N, \tag{77}$$

for $N < N_S$, with $1 < i < N$, and

$$\frac{dx_1^N}{dt} = N r_{N,B} x_N^N - (\bar{r}_{1,A} + T_A(\vec{x}))\, x_1^N, \tag{78}$$

$$\frac{dx_i^N}{dt} = (i-1)\bar{r}_{i-1,A} x_{i-1}^N - (i\bar{r}_{i,A} + T_A(\vec{x}))\, x_i^N, \tag{79}$$

$$\frac{dx_{N_S}^N}{dt} = (N_S - 1)\bar{r}_{N_S-1,A} x_{N_S-1}^N - (N_S r_{N_S,B} + T_B(\vec{x}))\, x_j^N, \tag{80}$$

$$\frac{dx_j^N}{dt} = (j-1) r_{j-1,B} x_{j-1}^N - (j r_{j,B} + T_B(\vec{x}))\, x_j^N, \tag{81}$$

$$\frac{dx_N^N}{dt} = (N-1) r_{N-1,B} x_{N-1}^N - T_B(\vec{x}) x_N^N, \tag{82}$$

for $N \geq N_S$, with $1 < i < N_S$ and $N_S \leq j < N$.

S3.4 Procedure for simulating evolutionary dynamics

To simulate the evolutionary dynamics dynamics, we repeatedly allow for rare multicellular mutants with different fragmentation sizes to arise and attempt to invade. For each invasion attempt, we simulate the resulting ecological dynamics, which, if invasion is successful, can lead to the displacement of the resident(s) by the invader or to coexistence. We wait for the ecological dynamics to reach steady state before introducing a new mutant. We continue doing so until an evolutionary stable community (ESC) is reached that cannot be invaded by any mutant.

In practice, we use simulations in which any life cycles with a maximum fragmentation size of 121 can appear. Mutations are assumed to be global (i.e., life cycles with fragmentation size $M+1$ can produce mutants of any other fragmentation size $1 \leq M' \leq 120$ with the same probability); our results stay qualitatively the same if the probability of mutations from M to M' decreases with $|M-M'|$). Only one life cycle type ($N+1$, $N\times 1$, or $N/2+N/2$) is allowed per simulation. The dynamic equations are chosen to match the life cycle type being simulated: equations (74)-(82) for $N+1$, equations (142)-(144) for $N\times 1$, and equations (161)-(166) for $N/2+N/2$. Although the introduction of mutants is stochastic, all simulations with the same set of parameters reach the same ESC. The full simulation code for this algorithm is at [1] and pseudocode is shown below.

(0) Initialize the simulation with a resident community $\vec{u}$ composed by the $1+1$ life cycle at steady state. That is, $u_1^1 = r_o/\gamma$ and $u_n^N = 0$ for $1 < N \leq 120$ and $1 \leq n \leq 120$;

(1) From all of the life cycles not present in the resident community, but able to either invade it or persist neutrally (i.e., $\rho(N) \geq 1$ for $1 \leq N \leq 120$), randomly chose one as the mutant;

(2) Set the initial condition for the ecological model as the current resident community at steady state ($\vec{x}(0) = \vec{u}$). Then, for $M+1$ being the mutant life cycle sampled in (2), add to the community mutant single cells equivalent to 1% of the total resident cell population: $x_1^M(0) = 0.01 \cdot \sum_{N\geq 1} \sum_{n=1}^{N} u_n^N$;

(3) Run the ecological model simulation numerically until $t = 5\cdot 10^7$, which is chosen large enough for the system to have reached steady state;

(4) Check for life cycles that have been excluded and drop them from the resident community: if $\rho(N) < 1$ for any N present in the ecological dynamics above, set $u_n^N = 0$ for all $1 \leq n \leq N$;

(5) In the new resident community $\vec{u}$, check if any life cycle is able to invade. That is, check if any $\rho(N) \geq 1$ for $1 \leq N \leq 120$ and N absent from $\vec{u}$;

(5.a) If the resident community $\vec{u}$ can be invaded, return to (1);

(5.a) Otherwise, if the resident community $\vec{u}$ cannot be invaded, move to (6);

(6) In the resident community $\vec{u}$, check for which $1 \leq N \leq 120$ it holds that $\rho(N) = 1$. The ESC is the collection of all of these life cycles.

S3.5 Simulation results

As described in the main text, we observe four different evolutionarily stable communities (ESCs) (main text Fig. 4 and Fig. 5). Here, we discuss these regimes in detail.

I. Coexistence and unbounded growth (blue region in main text Fig. 5a,b). When both layers are largely deprived of oxygen—that is, when N_U and N_L are low but $N_U > 0$—there are steep direct costs to group formation. Sinking life cycles can invade through escaping competition, but they do not displace the ancestor or the non-sinking life cycles that are neutral with it (i.e., non-sinking life cycles with fragmentation sizes at most $N_U + 1$; main text Fig. 4c, i). Over time, the benefits of escaping competition and the lack of any further costs of increasing group size allow the displacement of any resident sinking life cycle by larger ones—each one more effectively escaping competition by having more of its life stages in the lower layer (main text Fig. 4c, i). Although our simulations are limited to life cycles with fragmentation sizes up to $120 + 1$, we theoretically show that allowing the invasion of larger life cycles leads to a continued, unbounded increase in group size over evolutionary time (see Scenario 2 in section S4.3). Thus, the ESC for this scenario consists of a community of neutrally coexisting non-sinking life cycles that avoid oxygen deprivation and specialize on the upper layer and one sinking life cycle with a very high N that specializes on the lower layer. In reality, this N may ultimately be bounded if additional costs of group formation arise at larger group sizes.

II. Coexistence and bounded growth (green region in main text Fig. 5a,b). Further increase in the oxygen concentration eventually reverses the previous trend: sinking life cycles are now under selection for decreasing rather than increasing size (main text Fig. 4c, ii). This regime favors smaller group sizes because life cycles whose fragmentation size is only just above N_S are able to enjoy the benefits of escaping competition without paying the steep costs of oxygen-diffusion limitation that larger life cycles are subject to. Consequently, here the ESC consists of the smallest sinking life cycle (i.e., $N_S + 1$) in coexistence with all non-sinking life cycles that avoid the costs of oxygen deprivation.

III. Dominance of a single life cycle (yellow region in main text Fig. 5a,b). When higher oxygen concentrations diminish the costs of group formation even further, sufficiently small sinking life cycles become able to exert such a strong competitive pressure that they can displace the ancestor and any other non-sinking life cycles that are neutral with it (main text Fig. 4c, iii). The ESC now consists of only one life cycle. As in the previous regime, group sizes remain bounded. The life cycle that ultimately dominates is either $N_S + 1$ (the smallest life cycle that sinks), or, if it is possible to grow even further without oxygen deprivation (i.e., $N_L > N_S$), it is $N_L + 1$ (the largest life cycle that escapes competition while still avoiding oxygen deprivation).

IV. Broad coexistence (red regions in main text Fig. 5a,b). Eventually, as oxygen availability increases past a critical threshold $N_L \geq N^*$, we find a qualitatively different outcome. Life cycle $N^* + 1$ is the smallest one for which a majority of its cell population is in the lower layer. As a result, this life cycle, and any larger ones, can still invade (as long as they do not exceed size N_L), but they cannot displace life cycles smaller than life cycle $N^* + 1$ (see Section S7.4 in the SI for analytical support). Instead, they will establish coexistence through niche partitioning, the larger one specializing on the lower layer and the smaller one specializing on the upper layer (main text Fig. 4c, iv). Once coexistence is established, both layers of the water column are equally occupied, and so all cells face the same amount of competition, irrespective of whether they belong to groups in the upper or lower layer. Because there are also no differences in growth rate between cells in groups that avoid oxygen deprivation, the dynamics become completely neutral and ultimately give rise to an ESC comprising of all life cycles that avoid oxygen deprivation (main text Fig. 4c, iv). An interesting feature of this regime is that some life cycles, including the unicellular ancestor, may initially be displaced but eventually reinvade. Broad coexistence can arise whenever there are no growth rate differences within layers: in addition to observing it when oxygen is abundant ($N_L \geq N^*$), we also find it in the extreme cases when there is no oxygen in either layer ($N_U = N_L = 0$) and when there is abundant oxygen in the upper layer

but no oxygen in the lower layer ($N_U \geq N_S - 1$, $N_L = 0$). In the latter two scenarios, all life cycles ultimately coexist.

S3.6 Robustness analysis

Other types of life cycles

Our qualitative outcomes—diverse ecological regimes and a non-monotonic relationship between oxygen availability and group size—hold across all three life cycle types ($N+1$, $N \times 1$, and $N/2+N/2$; see Extended Data Fig. 2). However, the life cycles differ quantitatively in which regimes are present, on the regime boundaries and on the attained group sizes—reflecting differences in how effectively they explore the lower layer. Because sinking $N \times 1$ life cycles dissolve entirely into solitary cells upon reproduction (which immediately rise to the upper layer), they must reach larger sizes before fragmenting in order to effectively enjoy the benefits of sinking—relative to $N+1$. As a result, in regimes II and III, multicellular life cycles always grow larger than N_S, even at the cost of increased oxygen deprivation (Extended Data Fig. 2b.ii; but note that $N_S = 10$ for life cycle $N \times 1$). The $N/2+N/2$ life cycle also severely reduces group size upon fragmentation, leading to larger groups in regimes II and III for similar reasons (Extended Data Fig. 2c.ii). Unlike $N \times 1$, however, $N/2+N/2$ fragments into groups rather than single cells, which allows the fragments to reach the lower layer more efficiently than $N+1$. In particular, for $N \geq 2N_S$, the $N/2+N/2$ life cycle becomes entirely restricted to the lower layer. This greater efficiency enables the $N/2+N/2$ life cycle to reach the broad coexistence regime (IV) at lower oxygen concentrations (Extended Data Fig. 2c): less growth is needed before groups release the upper layer from competition. The restriction to the lower layer also eliminates regime I: groups no longer need to grow ever-larger to escape upper-layer competition, as growing to $N = 2N_S$ suffices (Extended Data Fig. 2c). Beyond this threshold, further growth confers no additional competitive benefit; life cycles with $N > 2N_S$ can only arise neutrally. This gives rise to a new regime when the lower layer is entirely oxygen-deprived ($N_L = 0$): all life cycles larger than $2N_S$ coexist neutrally at the ESC (Extended Data Fig. S2c, regime V).

Other values of r_o/r_f

Our results are also robust to changes in the fermentation growth rate r_f. When the cost of fermentation is sufficiently large (r_f well below r_o), the same four ESC regimes arise, though the boundaries between them shift depending on r_o/r_f (Extended Data Fig. 3). When the cost of fermentation is small (r_f close to r_o), a fifth regime emerges: several intermediate and all large life cycles coexist, but small life cycles are excluded (Extended Data Fig. 4, regime V). We consistently find the non-monotonic relationship between oxygen concentration and group size regardless of r_o/r_f and, consequently, regardless of whether this fifth regime is present (Extended Data Fig. 4a.iii, b.iii, and c.iii). A comprehensive mathematical analysis of the Proterozoic Ocean model further shows that regimes I–V exhaust all possible ESC types for the $N+1$ life cycle (see Section S4).

Mixing

Finally, we relax the assumption that there is perfect spatial segregation of single cells/groups above and below the sinking size N_S. In practice, segregation may be imperfect—for instance, single cells may occasionally lose buoyancy and sink to the lower layer, or single cells produced by groups in the lower layer may not immediately return to the upper layer. To relax this assumption, we now give single cells and groups smaller than N_S can access to the lower layer (see Section S3.3 for the mathematical details), while we still assume that large enough groups will always sink. We, thus, introduce a parameter $0 \leq q_L \leq 0.5$ to define the proportion of single cells and groups smaller than N_S that occupy the lower layer (before, we had $q_L = 0$).

We find that our results are qualitatively robust to low amounts of mixing (here approximately $q_L \leq 0.1$), for which we recover all four regions and the non-monotonic relationship between oxygen availability and group size (Extended Data Fig. 5a). However, as mixing increases and escaping competition from the unicellular ancestor becomes more difficult, it becomes possible that multicellularity fails to evolve altogether (with the exception of very small multicellular life cycles that are neutral with the ancestor; Extended Data Fig. 5a, gray region). In part of this region where we do not observe sinking multicellularity in the ESC, evolving sinking multicellularity is impossible altogether; in the other part, it can only evolve at very high fragmentation sezes, not captured in our simulations (Extended Data Fig. 5b). At maximum mixing ($q_L = 0.5$), non-trivial multicellularity can only evolve when there is enough oxygen to avoid oxygen deprivation altogether. Thus, as expected, indirectly beneficial multicellularity can only evolve if the environment is sufficiently heterogeneous. Nonetheless, at low mixing (here approximately $0 \leq q_L \leq 0.1$) we still recover all four regions and, as mixing increases towards moderate levels, only region I disappears. This result reinforces the robustness of our findings—including the non-monotonicity—at low to moderate mixing levels.

S4 Analytical results for the Proterozoic Ocean model

Here we perform an extensive mathematical analysis of the Proterozoic Ocean model for life cycles $N+1$:

- in S4.1 we derive invasion conditions that determine when life cycles can invade, depending on the current occupancy of both layers;
- in S4.2 we establish an auxiliary result on the spatial distribution of sufficiently large life cycles, which we will need for the classification of ESCs;
- in S4.3 we derive our main result, which is an exhaustive classification of the possible ESCs. This analysis confirms the diversity of ESCs observed in the main text (I-IV) and shows that no other ESCs are possible, aside from one additional ESC (V) which we indeed observe in the simulations performed for the robustness analysis (Extended Data Figure 4);
- in S4.4 we explain the successive dynamics that ultimately give rise to broad coexistence of all life cycles in regime IV, by focusing on the anoxic regime ($N_L = N_U = 0$).

In all these subsections, we assume that there is no mixing ($q_B = 0$). Finally, we present one analytical result for the scenario where mixing is allowed ($q_B > 0$):

- in Subsection S4.5 we derive conditions under which the unicellular ancestor can be invaded by large sinking life cycles when there is mixing between the layers.

S4.1 Invasion conditions

As before, we will make use of each life cycle's reproduction number. If $\rho(N)$ denotes the reproduction number of a life cycle $N+1$ then at steady state we know the following:

- if $\rho(N) > 1$, then $N+1$ is currently absent but would be able to invade;
- if $\rho(N) = 1$, then $N+1$ is either already present or would be able to invade neutrally;
- if $\rho(N) < 1$, then $N+1$ is currently absent and would not be able to invade.

We will next unpack these conditions in terms of the occupancy of each layers (T_A^* and T_B^*). We distinguish between non-sinking ($N < N_S$) and sinking ($N \geq N_S$) life cycles, and then, for each of these, we further distinguish between those that avoid oxygen deprivation and the ones that experience oxygen deprivation.

Non-sinking life cycles

The reproduction number of a non-sinking life cycle $N+1$ ($N < N_S$) is given by

$$\rho(N) = \frac{N r_f}{\gamma T_A^*} \prod_{1 \leq i \leq N_U} \frac{i r_o}{i r_o + \gamma T_A^*} \prod_{N_U < i < N} \frac{i \bar{r}_i}{i \bar{r}_i + \gamma T_A^*}, \tag{83}$$

where

$$\bar{r}_i = \begin{cases} r_o & \text{for } i \leq N_U, \\ \dfrac{N_U \cdot r_o + (i - N_U) \cdot r_f}{i} & \text{for } i > N_U. \end{cases} \tag{84}$$

Note that $\rho(N)$ is a decreasing function of T_A^*. If $N \leq N_U$, then the life cycle completely avoids oxygen deprivation. In this case, we see that $\rho(N) = 1$ corresponds to $T_A^* = \frac{r_o}{\gamma}$. After all, if $T_A^* = \frac{r_o}{\gamma}$ and $N \leq N_U$, then (83) simplifies to

$$\rho(N) = \frac{N r_o}{\gamma \cdot \frac{r_o}{\gamma}} \prod_{1 \leq i < N} \frac{i r_o}{i r_o + \gamma \cdot \frac{r_o}{\gamma}} = N \prod_{1 \leq i < N} \frac{i}{i+1} = 1. \tag{85}$$

Therefore, non-sinking life cycles that avoid oxygen deprivation are present (or can invade neutrally) if $T_A^* = \frac{r_o}{\gamma}$; are absent and can invade if $T_A^* < \frac{r_o}{\gamma}$; and are absent and cannot invade if $T_A^* > \frac{r_o}{\gamma}$.

Result S4.1: Invasion of non-sinking life cycles that avoid oxygen deprivation

A non-sinking life cycle that avoids oxygen deprivation (i.e., a life cycle $N+1$ with $N \leq N_U$) can invade if and only if $T_A^* \leq \frac{r_o}{\gamma}$.

We can also interpret Result S4.1 visually: in (T_A^*, T_B^*)-space, the communities that can be invaded by a non-sinking life cycle that avoids oxygen deprivation are those to the left of the vertical line $T_A^* = \frac{r_o}{\gamma}$ (Supplementary Figure 2, left).

For non-sinking life cycles that experience oxygen deprivation, we have the following result.

Result S4.2: Non-sinking life cycles that experience oxygen deprivation

Non-sinking life cycles that experience oxygen deprivation can never be part of an evolutionarily stable community.

Indeed, for $N_U \leq N, N+1 < N_S$, we deduce from (83) that the ratio between reproduction numbers $\frac{\rho(N+1)}{\rho(N)}$ is equal to

$$\frac{\rho(N+1)}{\rho(N)} = \frac{N+1}{N} \cdot \frac{N \bar{r}_N}{N \bar{r}_N + \gamma T_A^*} = \frac{N+1}{N + \frac{\gamma T_A^*}{\bar{r}_N}}. \tag{86}$$

For $T_A^* = \frac{r_o}{\gamma}$, we find that $\frac{\rho(N+1)}{\rho(N)} < 1$ (because $r_o > \bar{r}_N$) so $\rho(N+1) < \rho(N)$. Therefore, if the non-sinking life cycles that avoid oxygen deprivation are present (meaning that they have reproduction number 1 and $T_A^* = \frac{r_o}{\gamma}$), then non-sinking life cycles that experience oxygen deprivation cannot invade. Conversely, if any non-sinking life cycle that faces oxygen deprivation is present at steady state, we must have $T_A^* < \frac{r_o}{\gamma}$, which means that the non-sinking life cycles that avoid oxygen deprivation can invade. We conclude that a non-sinking life cycle that faces oxygen deprivation can never be present in an evolutionarily stable community; therefore, in what follows, we exclude these life cycles from the analysis.

Sinking life cycles

For a sinking life cycle $N+1$ with $N \geq N_S$, the reproduction number is equal to

$$\rho(N) = \frac{N\bar{r}_N}{\gamma T_B^*} \prod_{1 \leq i < N_S} \frac{i\bar{r}_i}{i\bar{r}_i + \gamma T_A^*} \prod_{N_S \leq i < N} \frac{i\bar{r}_i}{i\bar{r}_i + \gamma T_B^*}, \tag{87}$$

where

$$\bar{r}_i = \begin{cases} r_o, & \text{for } i \leq N_U, \\ \dfrac{N_U \cdot r_o + (i - N_U) \cdot r_f}{i}, & \text{for } N_U < i < N_S, \\ r_o, & \text{for } N_S \leq i \leq N_L, \\ \dfrac{N_L \cdot r_o + (i - N_L) \cdot r_f}{i}, & \text{for } i > N_L \text{ and } i \geq N_S. \end{cases} \tag{88}$$

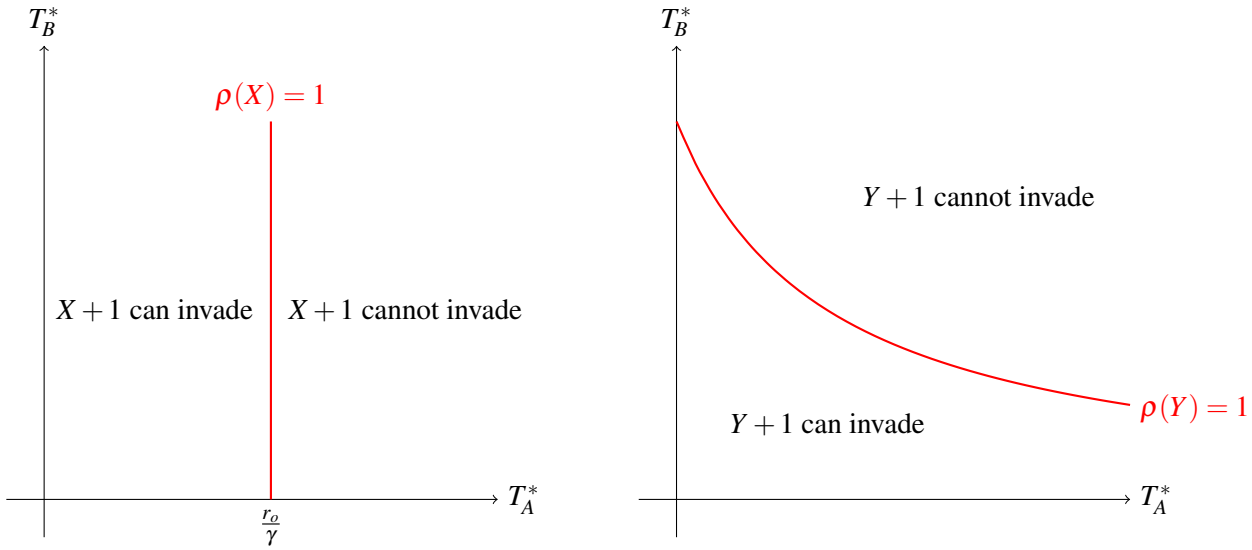

Supplementary Figure 2: Invasion boundaries for non-sinking life cycles $X+1$ that avoid oxygen deprivation (left) and sinking life cycles $Y+1$ (right).

Because $\rho(N)$ is a decreasing function of both T_A^* and T_B^*, the invasion boundary $\rho(N) = 1$ is a curve in (T_A^*, T_B^*)-space below which $N+1$ can invade and above which it cannot (Supplementary Figure 2, right). The following result describes the shape of this curve.

Result S4.3: Shape of the invasion boundary of a sinking life cycle

A sinking life cycle $N+1$ can invade if and only if (T_A^*, T_B^*) lies below the invasion boundary $\rho(N) = 1$. This invasion boundary is decreasing and convex.

To see this, note that the equation $\rho(N) = 1$ is equivalent to

$$1 = \frac{N\bar{r}_N}{\gamma T_B^*} \prod_{1 \le i \le N_S} \frac{i\bar{r}_i}{i\bar{r}_i + \gamma T_A^*} \prod_{N_S \le i < N} \frac{i\bar{r}_i}{i\bar{r}_i + \gamma T_B^*} \tag{89}$$

or

$$\gamma T_B^* \prod_{1 \le i < N_S} (i\bar{r}_i + \gamma T_A^*) \prod_{N_S \le i < N} (i\bar{r}_i + \gamma T_B^*) = N! \cdot \prod_{i=1}^{N} \bar{r}_i. \tag{90}$$

We take the logarithm and differentiate with respect to T_A^* to obtain

$$\sum_{1 \le i < N_S} \frac{\gamma}{i\bar{r}_i + \gamma T_A^*} + \frac{dT_B^*}{dT_A^*} \cdot \left(\frac{1}{T_B^*} + \sum_{N_S \le i < N} \frac{\gamma}{i\bar{r}_i + \gamma T_B^*} \right) = 0. \tag{91}$$

The slope of the invasion boundary is therefore given by the implicit derivative

$$\frac{dT_B^*}{dT_A^*} = -\frac{\displaystyle\sum_{1 \le i < N_S} \frac{\gamma}{i\bar{r}_i + \gamma T_A^*}}{\displaystyle\frac{1}{T_B^*} + \sum_{N_S \le i < N} \frac{\gamma}{i\bar{r}_i + \gamma T_B^*}}. \tag{92}$$

From this equation we immediately see that (1) $\frac{dT_B^*}{dT_A^*}$ is negative, so the invasion boundary is decreasing; and (2) $\frac{dT_B^*}{dT_A^*}$ is an increasing function of T_A^* (where we use that, along the invasion boundary, T_B^* is a decreasing function of T_A^*; therefore, the denominator of (92) is an increasing function of T_A^*), so the invasion boundary is indeed convex.

The next two results address the relative positioning of the invasion boundaries of sinking life cycles.

Result S4.4: Intersection of invasion boundaries of sinking life cycles that avoid oxygen deprivation

Consider two sinking life cycles $Y+1$ and $Z+1$ (with $Z > Y$) that avoid oxygen deprivation ($Z \le N_L$). Then, the invasion boundary $\rho(Y) = 1$ lies above the invasion boundary $\rho(Z) = 1$ above the line $T_B^* = \frac{r_o}{\gamma}$, and below it below this line (see Supplementary Figure 3). In particular, the invasion boundaries $\rho(Y) = 1$ and $\rho(Z) = 1$ intersect in a point on the line $T_B^* = \frac{r_o}{\gamma}$; this is the point $(T_A^*, T_B^*) = (\frac{r_o}{\gamma}, \frac{r_o}{\gamma})$.

Note that Result S4.4 immediately implies that the invasion boundaries of *all* sinking life cycles that avoid oxygen deprivation pass through the point $(\frac{r_o}{\gamma}, \frac{r_o}{\gamma})$.

To establish Result S4.4, we first note that we may assume that $Z - Y = 1$ (i.e., the life cycle $Z+1$ has only one more life stage than $Y+1$); this will automatically imply the result for bigger values of $Z-Y$. When $Z - Y = 1$, the reproduction numbers $\rho(Z)$ and $\rho(Y)$ (which are given by (87) for $N \le N_L$) are related via

$$\frac{\rho(Y+1)}{\rho(Y)} = \frac{\dfrac{(Y+1)r_o}{\gamma T_B^*} \cdot \dfrac{Yr_o}{Yr_o + \gamma T_B^*}}{\dfrac{Yr_o}{\gamma T_B^*}} = \frac{(Y+1)r_o}{Yr_o + \gamma T_B^*} = \frac{Yr_o + r_o}{Yr_o + \gamma T_B^*}, \tag{93}$$

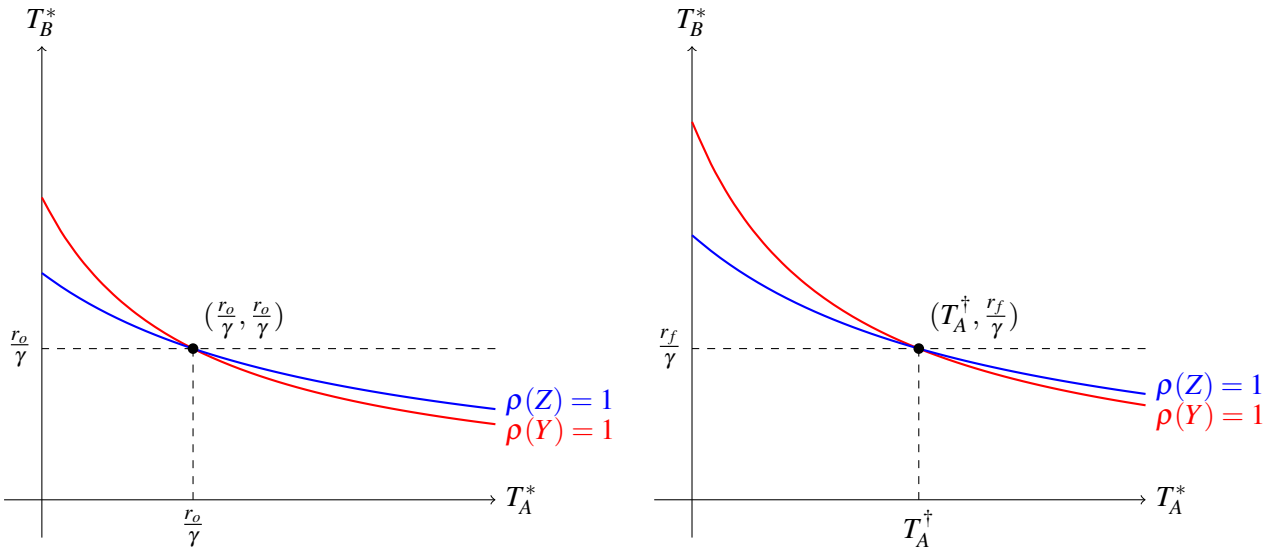

Supplementary Figure 3: Invasion boundaries of sinking life cycles that avoid oxygen deprivation (left) and that experience oxygen deprivation (right). In both scenarios, all invasion boundaries intersect at a single point on the line $T_B^* = \frac{r_o}{\gamma}$ (left) or $T_B^* = \frac{r_f}{\gamma}$ (right).

We now see that for $T_B^* = \frac{r_o}{\gamma}$ we have $\rho(Z) = \rho(Y)$, so the invasion boundaries $\rho(Y) = 1$ and $\rho(Z) = 1$ intersect on the line $T_B^* = \frac{r_o}{\gamma}$; for $T_B^* > \frac{r_o}{\gamma}$ we have $\rho(Z) < \rho(Y)$, so the invasion boundary $\rho(Y) = 1$ lies above the invasion boundary $\rho(Z) = 1$; and for $T_B^* < \frac{r_o}{\gamma}$ we have $\rho(Z) > \rho(Y)$, implying the opposite. Finally, to see that the point of intersection is $(T_A^*, T_B^*) = (\frac{r_o}{\gamma}, \frac{r_o}{\gamma})$, note that (87) becomes 1 for $N \leq N_L$ $(\leq N_U)$ and $T_A^* = T_B^* = \frac{r_o}{\gamma}$.

For the sinking life cycles that experience oxygen deprivation we obtain a similar result.

Result S4.5: Intersection of invasion boundaries of sinking life cycles that experience oxygen deprivation

Consider two sinking life cycles $Y+1$ and $Z+1$ (with $Z > Y$) that experience oxygen deprivation ($Y > N_L$). Then the invasion boundary $\rho(Y) = 1$ lies above the invasion boundary $\rho(Z) = 1$ above the line $T_B^* = \frac{r_f}{\gamma}$, and below it below this line (see Supplementary Figure 3). In particular, the invasion boundaries $\rho(Y) = 1$ and $\rho(Z) = 1$ intersect in a point $(T_A^*, T_B^*) = (T_A^\dagger, \frac{r_f}{\gamma})$ on the line $T_B^* = \frac{r_f}{\gamma}$.

Note that Result S4.5 immediately implies that the invasion boundaries of *all* sinking life cycles that experience oxygen deprivation pass through the point $(T_A^\dagger, \frac{r_f}{\gamma})$.

As before, we first note that we may assume that $Z - Y = 1$ and note that the reproduction numbers $\rho(Z)$

and $\rho(Y)$ (given by (87) for $N > N_L$) are related via

$$\frac{\rho(Y+1)}{\rho(Y)} = \frac{\frac{(Y+1)\bar{r}_{Y+1}}{\gamma T_B^*} \cdot \frac{Y\bar{r}_Y}{Y\bar{r}_Y + \gamma T_B^*}}{\frac{Y\bar{r}_Y}{\gamma T_B^*}} = \frac{(Y+1)\bar{r}_{Y+1}}{Y\bar{r}_Y + \gamma T_B^*} = \frac{Y\bar{r}_Y + r_f}{Y\bar{r}_Y + \gamma T_B^*}, \tag{94}$$

where we use that $(i+1)\bar{r}_{i+1} = i\bar{r}_i + r_f$ for $i > N_S$ (see (88)). We now see that for $T_B^* = \frac{r_f}{\gamma}$ we have $\rho(Z) = \rho(Y)$, so the invasion boundaries $\rho(Y) = 1$ and $\rho(Z) = 1$ intersect on the line $T_B^* = \frac{r_f}{\gamma}$; for $T_B^* > \frac{r_f}{\gamma}$ we have $\rho(Z) < \rho(Y)$, so the invasion boundary $\rho(Y) = 1$ lies above the invasion boundary $\rho(Z) = 1$; and for $T_B^* < \frac{r_f}{\gamma}$ we have $\rho(Z) > \rho(Y)$, implying the opposite. Then, we define $T_A^\dagger$ as the value for T_A^* such that $(T_A^*, T_B^*) = (T_A^\dagger, \frac{r_f}{\gamma})$ lies on the invasion boundary of all sinking life cycles that experience oxygen deprivation.

Finally, we examine the largest sinking life cycle that avoids oxygen deprivation $N_L + 1$, which exists only if $N_L \geq N_S$.

Result S4.6: Intersections of the invasion boundary of life cycle $N_L + 1$

The invasion boundary of the sinking life cycle $N_L + 1$ ($N_L \geq N_S$) passes through both:

- The intersection point $(T_A^*, T_B^*) = (\frac{r_o}{\gamma}, \frac{r_o}{\gamma})$ of the invasion boundaries of all sinking life cycles that avoid oxygen deprivation;
- The intersection point $(T_A^*, T_B^*) = (T_A^\dagger, \frac{r_f}{\gamma})$ of all sinking life cycles that experience oxygen deprivation.

Additionally, the invasion boundary $\rho(N_L) = 1$ lies above the invasion boundaries of larger sinking life cycles above the line $T_B^* = \frac{r_f}{\gamma}$, and below them below this line.

The fact the invasion boundary of $N_L + 1$ passes through $(T_A^*, T_B^*) = (\frac{r_o}{\gamma}, \frac{r_o}{\gamma})$ is a special case of Result S4.4. The remaining statements follow from noting that the logic of Result S4.5 also applies with $Y = N_L$.

S4.2 Spatial distribution of sufficiently large life cycles in isolation

In this section, we establish an auxiliary result on the spatial distribution of sufficiently large life cycles in isolation. We will use it in the next section to classify ESCs.

Result S4.7: Spatial distribution of sufficiently large life cycles in isolation

For all sufficiently large N it is impossible for the sinking life cycle $N + 1$ to exist in isolation at a steady state with $T_B^* \leq \frac{r_f}{\gamma}$ and $T_A^* \geq \frac{r_o}{\gamma}$.

To establish Result S4.7, we will first establish a lower bound for T_B^* and an upper bound for T_A^* that only depends on the population composition through one life stage, x_{N_S-1}.

To establish the bound on T_B^*, we recall that

$$\dot{x}_i = (i-1)\bar{r}_{i-1}x_{i-1} - i\bar{r}_i x_i - \gamma T_B \overline{x_i} \tag{95}$$

for $N_S \leq i < N$. If $N+1$ exists at a steady state with $T_B^* \leq \frac{r_f}{\gamma}$, we therefore find that

$$x_i = \frac{(i-1)\bar{r}_{i-1}x_{i-1}}{i\bar{r}_i + \gamma T_B^*} \geq \frac{(i-1)\bar{r}_{i-1}}{(i+1)\bar{r}_i} \cdot x_{i-1}, \tag{96}$$

where we have used that $\gamma T_B^* \leq r_f \leq \bar{r}_i$. For $N_S \leq j < N$ we now obtain

$$\frac{x_j}{x_{N_S-1}} = \prod_{i=N_S}^{j} \frac{x_i}{x_{i-1}} \geq \prod_{i=N_S}^{j} \frac{i-1}{i+1} \cdot \prod_{i=N_S}^{j} \frac{\bar{r}_{i-1}}{\bar{r}_i} = \frac{(N_S-1)N_S}{j(j+1)} \cdot \frac{\bar{r}_{N_S}}{\bar{r}_j} \geq \frac{(N_S-1)N_S}{j(j+1)} \cdot \frac{r_f}{r_o}, \tag{97}$$

which leads to the estimate

$$T_B^* = \sum_{j=N_S}^{N} j x_j > \sum_{j=N_S}^{N-1} j x_j \geq x_{N_S-1} \cdot (N_S-1)N_S \cdot \frac{r_f}{r_o} \cdot \sum_{j=N_S}^{N-1} \frac{1}{j+1}. \tag{98}$$

To obtain an upper bound on T_A^*, we first note that the change in the total number of cells $T_A + T_B$ is equal to

$$\frac{d(T_A+T_B)}{dt} = r_A T_A + r_B T_B - \gamma(T_A^2 + T_B^2), \tag{99}$$

where $r_A = \frac{1}{T_A}\sum_{i=1}^{N_S-1} i x_i \bar{r}_i \leq r_o$ is the average reproduction rate of cells in the upper layer and, similarly, $r_B \leq r_o$ is the average reproduction rate of cells in the lower layer. At steady state, we know that

$$\gamma\left(T_A^{*2} + T_B^{*2}\right) = r_A T_A^* + r_B T_B^* \leq r_o(T_A^* + T_B^*). \tag{100}$$

Under the assumption that $T_A^* \geq \frac{r_o}{\gamma}$ and $T_B^* \geq \frac{r_f}{\gamma}$ we have $T_A^* \geq T_B^*$, and so it follows that

$$\gamma T_A^{*2} \leq \gamma\left(T_A^{*2} + T_B^{*2}\right) \leq r_o(T_A^* + T_B^*) \leq 2r_o T_A^*, \tag{101}$$

which implies $T_A^* \leq \frac{2r_o}{\gamma}$. For $2 \leq i < N_S$ we have

$$\dot{x}_i = (i-1)\bar{r}_{i-1}x_{i-1} - i\bar{r}_i x_i - \gamma T_A x_i, \tag{102}$$

and, therefore, at steady state we know that

$$\frac{x_i}{x_{i-1}} = \frac{(i-1)\bar{r}_{i-1}}{i\bar{r}_i + \gamma T_A^*} \geq \frac{(i-1)\bar{r}_{i-1}}{i\bar{r}_i + 2r_o} \geq \frac{(i-1)r_f}{(i+2)r_o}. \tag{103}$$

For $1 \leq j \leq N_S - 1$ we therefore obtain

$$\frac{x_{N_S-1}}{x_j} = \prod_{i=j+1}^{N_S-1} \frac{x_i}{x_{i-1}} \geq \prod_{i=j+1}^{N_S-1} \frac{i-1}{i+2} \prod_{i=j+1}^{N_S-1} \frac{r_f}{r_o} > \frac{j}{N_S^3} \cdot \left(\frac{r_f}{r_o}\right)^{N_S}. \tag{104}$$

This leads to the estimate

$$T_A^* = \sum_{j=1}^{N_S-1} j x_j = x_{N_S-1} \sum_{j=1}^{N_S-1} \frac{j x_j}{x_{N_S-1}} < x_{N_S-1} N_S^4 \left(\frac{r_o}{r_f}\right)^{N_S}. \tag{105}$$

Equations (98) and (105) tell us that there exist positive constants C_A and C_B (which only depend on N_S, r_f, and r_o) such that

$$\frac{T_B^*}{x_{N_S}-1} \geq C_B \cdot \sum_{j=N_S}^{N-1} \frac{1}{j+1} \qquad \text{and} \qquad \frac{T_A^*}{x_{N_S}-1} < C_A. \tag{106}$$

Therefore, if $T_A^* \geq \frac{r_o}{\gamma}$ and $T_B^* \leq \frac{r_f}{\gamma}$, it would follow that

$$\frac{r_o}{r_f} \geq \frac{T_B^*}{T_A^*} > \frac{C_B}{C_A} \cdot \sum_{j=N_S}^{N-1} \frac{1}{j+1}. \tag{107}$$

Because the harmonic series diverges, (107) can only hold for sufficiently small N. Therefore, Result S4.7 holds.

S4.3 Classification of ESCs

There are multiple ESCs possible, depending on the parameters N_U, N_L, N_S, r_o, and r_f. Here, we will provide a full classification of the communities that can arise as ESC. Our main result is as follows.

Result S4.8: ESC classification

The following is an exhaustive list of all possible ESCs:

- Coexistence of non-sinking life cycles that avoid oxygen deprivation with a single sinking life cycle subject to selection for increasing size (only when $N_L < N_S$; main text regime I);
- Coexistence of non-sinking life cycles that avoid oxygen deprivation with the smallest sinking life cycle N_S+1 (only when $N_L < N_S$; main text regime II);
- Dominance of the smallest sinking life cycle N_S+1 (if $N_L < N_S$) or the smallest sinking life cycle that avoids oxygen deprivation N_L+1 (if $N_L \geq N_S$) (main text regime III);
- Coexistence of all life cycles (if $N_L < N_S$) or coexistence of all life cycles that avoid oxygen deprivation (if $N_L \geq N_S$) (main text regime IV);
- Coexistence of all sinking life cycles (if $N_L < N_S$) or all sinking life cycles starting at N_L+1 (if $N_L \geq N_S$) (regime V in the robustness analysis, Extended Data Figure 4).

We will obtain Result S4.8 by distinguishing a number of scenarios depending on whether $N_L < N_S$ (i.e., whether or not there are sinking life cycles that avoid oxygen deprivation) and the value of $T_A^\dagger$. Recall that $T_A^\dagger$ is defined as the value for T_A^* such that $(T_A^*, T_B^*) = (T_A^\dagger, \frac{r_f}{\gamma})$ lies on the invasion boundary of all sinking life cycles that experience oxygen deprivation (Result S4.5).

In particular, when $N_L < N_S$, then $(T_A^\dagger, \frac{r_f}{\gamma})$ lies on the invasion boundary of the smallest sinking life cycle

N_S+1. This means that

$$1=\rho(N_S) \qquad \text{(evaluated at } (T_A^*,T_B^*)=(T_A^\dagger,\tfrac{r_f}{\gamma})) \tag{108}$$

$$=\frac{N_S\bar{r}_{N_S}}{\gamma\cdot\frac{r_f}{\gamma}}\cdot\prod_{1\le i<N_S}\frac{i\bar{r}_i}{i\bar{r}_i+\gamma T_A^\dagger} \tag{109}$$

$$=\frac{\bar{r}_{N_S}}{r_f}\cdot\prod_{1\le i<N_S}\frac{i+1}{i+\frac{\gamma T_A^\dagger}{\bar{r}_i}} \tag{110}$$

On the other hand, when $N_L\ge N_S$, then $(T_A^\dagger,\frac{r_f}{\gamma})$ lies on the invasion boundary of the life cycle $(N_L+1)+1$. In that case, we obtain

$$1=\rho(N_L+1) \qquad \text{(evaluated at } (T_A^*,T_B^*)=(T_A^\dagger,\tfrac{r_f}{\gamma})) \tag{111}$$

$$=\frac{(N_L+1)\bar{r}_{N_L+1}}{\gamma\cdot\frac{r_f}{\gamma}}\cdot\prod_{1\le i<N_S}\frac{ir_o}{ir_o+\gamma T_A^\dagger}\prod_{N_S\le i<N_L+1}\frac{ir_o}{ir_o+\gamma(\frac{r_f}{\gamma})} \tag{112}$$

$$=\frac{\bar{r}_{N_L+1}}{r_f}\cdot\prod_{1\le i<N_S}\frac{i+1}{i+\frac{\gamma T_A^\dagger}{r_o}}\prod_{N_S\le i<N_L+1}\frac{i+1}{i+\frac{r_f}{r_o}} \tag{113}$$

We can use these equations to derive some simple properties of $T_A^\dagger$:

Result S4.9: Properties of $T_A^\dagger$

The threshold $T_A^\dagger$ has the following properties:

(i) $T_A^\dagger\ge\frac{r_f}{\gamma}$ for $N_L<N_S$, with equality only if $N_U=0$;

(ii) $T_A^\dagger>\frac{r_o}{\gamma}$ for $N_L\ge N_S$;

To establish (i), we see that substituting $T_A^\dagger=\frac{r_f}{\gamma}$ in (110) would make the right hand side bigger than 1 (unless $\bar{r}_i=r_f$ for all i, which happens only when $N_U=0$). Similarly, to establish (ii), we see that $T_A^\dagger\le\frac{r_o}{\gamma}$ would imply that

$$\frac{N_Lr_o+r_f}{r_f}\cdot\prod_{1\le i<N_S}\underbrace{\frac{ir_o}{ir_o+\gamma T_A^\dagger}}_{\ge\frac{i}{i+1}}\prod_{N_S\le i<N_L+1}\underbrace{\frac{ir_o}{ir_o+r_f}}_{>\frac{i}{i+1}}\ge\frac{N_Lr_o+r_f}{r_f}\prod_{1\le i<N_L+1}\frac{i}{i+1}=\frac{N_Lr_o+r_f}{(N_L+1)r_f}>1, \tag{114}$$

contradicting (113).

In light of Result S4.9, we will distinguish five scenarios:

- Scenario 1: $N_L<N_S$, $T_A^\dagger=\frac{r_f}{\gamma}$;
- Scenario 2: $N_L<N_S$, $\frac{r_f}{\gamma}<T_A^\dagger<\frac{r_o}{\gamma}$;

- Scenario 3: $N_L < N_S$, $T_A^\dagger = \frac{r_o}{\gamma}$;
- Scenario 4: $N_L < N_S$, $T_A^\dagger > \frac{r_o}{\gamma}$;
- Scenario 5: $N_L \geq N_S$, $T_A^\dagger > \frac{r_o}{\gamma}$.

Because (110) and (113) imply that $T_A^\dagger$ is an increasing function of N_U, N_L, and $\frac{r_o}{r_f}$, we can think of these scenarios as corresponding to gradually increasing oxygen concentrations.

We will now analyze Scenarios 1-5 one by one and determine the possible ESCs for each. In doing so, we repeatedly use that in (T_A^*, T_B^*)-space, the ESC must correspond to a point that lies on the invasion boundaries of all life cycles that are present in the ESC and above the invasion boundaries of all other life cycles.

Scenario 1: $N_L < N_S$, $T_A^\dagger = \frac{r_f}{\gamma}$

The first scenario corresponds to a completely anoxic world ($N_U = 0$, or, equivalently, $r_o = r_f$). In this case, the invasion boundary of all non-sinking life cycles is the vertical line $T_A^* = \frac{r_f}{\gamma}$ (Supplementary Figure 4a). The invasion boundaries of all life cycles (non-sinking or sinking) intersect at the point $(\frac{r_f}{\gamma}, \frac{r_f}{\gamma})$ (Supplementary Figure 4a). We see that evolutionarily stable communities cannot exist to the left of the line $T_A^* = \frac{r_f}{\gamma}$, because then non-sinking life cycles could invade. Moreover, evolutionarily stable communities also cannot exist to the right of the line $T_A^* = \frac{r_f}{\gamma}$: the only communities that can exist there consist of sinking life cycles in isolation; however, these life cycles can be displaced by bigger life cycles, and once these life cycles are sufficiently large, they cannot exist in the shaded region anymore by Result S4.7. Therefore, the ESC must satisfy $T_A^* = \frac{r_f}{\gamma}$. Because non-sinking life cycles can be invaded by sinking life cycles, the ESC must in fact correspond to the point $(T_A^*, T_B^*) = (\frac{r_f}{\gamma}, \frac{r_f}{\gamma})$, where all life cycles can coexist (Supplementary Figure 4a, red point). Therefore, the ESC for Scenario 1 consists of all life cycles. In Section S4.4 we analyze the evolutionary dynamics that give rise to this ESC in more detail.

Scenario 2: $N_L < N_S$, $\frac{r_f}{\gamma} < T_A^\dagger < \frac{r_o}{\gamma}$

In the second scenario, the invasion boundaries of sinking life cycles intersect to the left of the invasion boundary of non-sinking life cycles (Supplementary Figure 4b). We first observe that there cannot be an ESC with $T_B^* \geq \frac{r_f}{\gamma}$. Such an ESC would lie to the left of the invasion boundary of non-sinking life cycles and therefore non-sinking life cycles would be able to invade it. For $T_B^* < \frac{r_f}{\gamma}$, we know that sinking life cycles can always be invaded by larger sinking life cycles (Result S4.5). Therefore, in this case there is no true ESC: sinking life cycles will continually be displaced by larger and larger sinking life cycles. Finally, from Result S4.7 it follows that the shaded region in Supplementary Figure 4b cannot contain sufficiently large sinking life cycles in isolation; this tells us that the ESC cannot exist to the right of the invasion boundary of non-sinking life cycles and therefore that non-sinking life cycles will be present in the ESC. Altogether, we recover regime I from the main text: the ESC contains of non-sinking life cycles that avoid oxygen deprivation and a single sinking life cycle that is subject to selection for increasing size.

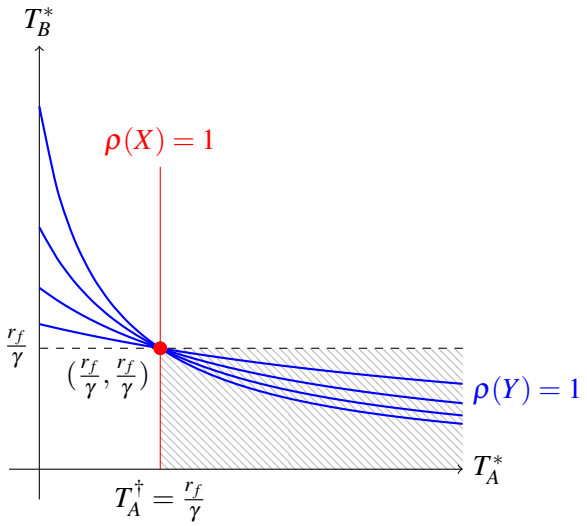

(a) Scenario 1: $T_A^\dagger = \frac{r_f}{\gamma}$

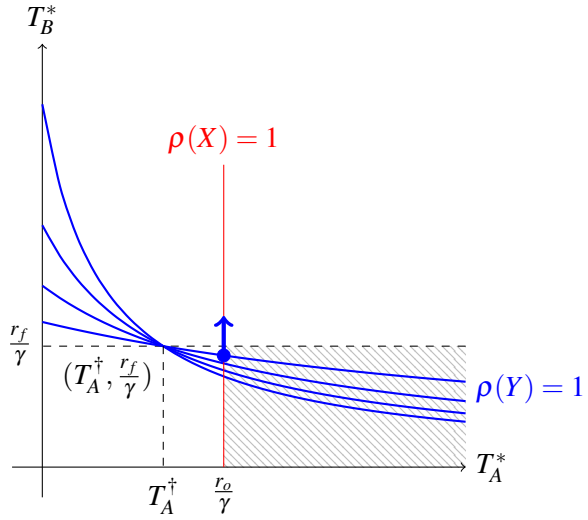

(b) Scenario 2: $\frac{r_f}{\gamma} < T_A^\dagger < \frac{r_o}{\gamma}$

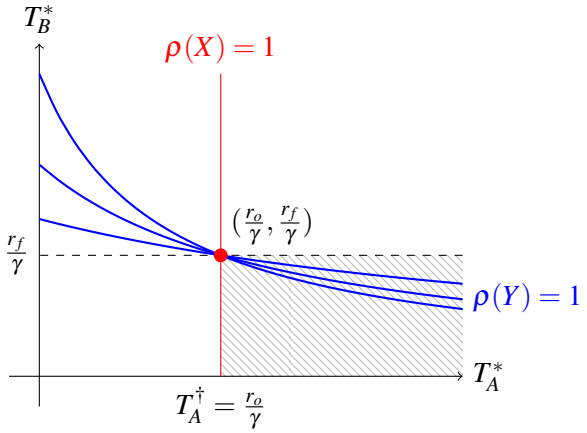

(c) Scenario 3: $T_A^\dagger = \frac{r_o}{\gamma}$

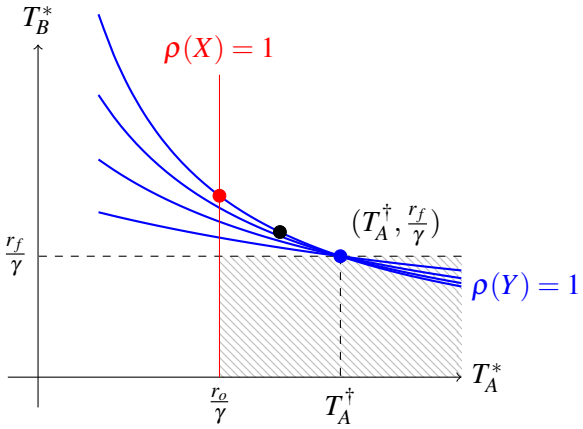

(d) Scenario 4: $T_A^\dagger > \frac{r_o}{\gamma}$

Supplementary Figure 4: Invasion boundaries and ESCs for $N_L < N_S$. The red line is the invasion boundary of non-sinking life cycles $X+1$ that avoid oxygen deprivation. The blue lines are the invasion boundaries of sinking life cycles $Y+1$. The shaded region cannot contain any sufficiently large life cycles in isolation, because of Result S4.7. Points indicate possible ESCs: coexistence of all life cycles (red point, Scenario 1 and 3; regime IV in the main text), coexistence of all non-sinking life cycles that avoid oxygen deprivation and a single sinking life cycle subject to selection for increasing size (blue point with arrow, Scenario 2; regime I in the main text); coexistence of all non-sinking life cycles that avoid oxygen deprivation and the smallest sinking life cycle N_S+1 (red point, Scenario 4; regime II in the main text); dominance of the smallest sinking life cycle N_S+1 (black point, Scenario 4; regime III in the main text); coexistence of all sinking life cycles (blue point, Scenario 4; regime V in the robustness analysis).

Scenario 3: $N_L < N_S$, $T_A^\dagger = \frac{r_o}{\gamma}$

In the third scenario, the invasion boundaries of sinking life cycles intersect exactly on the invasion boundary of non-sinking life cycles (Supplementary Figure 4c). Following similar arguments as in Scenario 1, there cannot be an ESC for $T_A^* < \frac{r_o}{\gamma}$ or in the shaded region in Supplementary Figure 4c. Thus, we can conclude that the only possible ESC is the coexistence of all sinking and non-sinking life cycles at $(T_A^*, T_B^*) = (\frac{r_o}{\gamma}, \frac{r_f}{\gamma})$.

A special case where $T_A^\dagger = \frac{r_o}{\gamma}$ always holds is when $N_U > N_S$ and $N_L = 0$, because then (110) implies $T_A^\dagger = \frac{r_o}{\gamma}$. Indeed, in our simulations, we consistently observe coexistence of all life cycles when $N_U > N_S$ and $N_L = 0$ (Fig. 5, main text).

Scenario 4: $N_L < N_S$, $T_A^\dagger > \frac{r_o}{\gamma}$

In the fourth scenario, the invasion boundaries of sinking life cycles intersect to the right of the invasion boundary of non-sinking life cycles (Supplementary Figure 4d). A similar argument reveals that there are three ESCs possible:

- Coexistence of non-sinking life cycles with the smallest possible sinking life cycle $N_S + 1$ (Supplementary Figure 4d, red point). This corresponds to regime II in the main text.
- Dominance of the smallest possible sinking life cycle $N_S + 1$ (Supplementary Figure 4d, black point). This corresponds to regime III in the main text.
- Coexistence of all sinking life cycles (Supplementary Figure 4d, blue point). We do not see this ESC for the parameter values in the main text, but it appears in our robustness analysis (regime V in Extended Data Figure 4).

Scenario 5: $N_L \geq N_S$, $T_A^\dagger > \frac{r_o}{\gamma}$

When $N_L \geq N_S$, the invasion boundaries of all sinking life cycles that avoid oxygen deprivation intersect at $(T_A^*, T_B^*) = \left(\frac{r_o}{\gamma}, \frac{r_o}{\gamma}\right)$ (red point in Supplementary Figure 5; see Result S4.4). Moreover, by Results S4.5 and S4.6, the invasion boundary of life cycle $N_L + 1$ intersects the invasion boundary of all sinking life cycles that experience oxygen deprivation at $(T_A^*, T_B^*) = \left(T_A^\dagger, \frac{r_f}{\gamma}\right)$ (blue point in Supplementary Figure 5). We therefore conclude that no ESCs can occur to the left of $T_A^* = \frac{r_o}{\gamma}$, since non-sinking life cycles can invade, nor to the right of $T_A^* = T_A^\dagger$, since this region (shaded in Supplementary Figure 5) is under selection for increasing size, yet no sufficiently large life cycle can exist there in isolation (Result S4.7). Therefore, only three ESCs are possible:

- coexistence of all life cycles that avoid oxygen deprivation (Supplementary Figure 5, red point; regime IV in the main text);

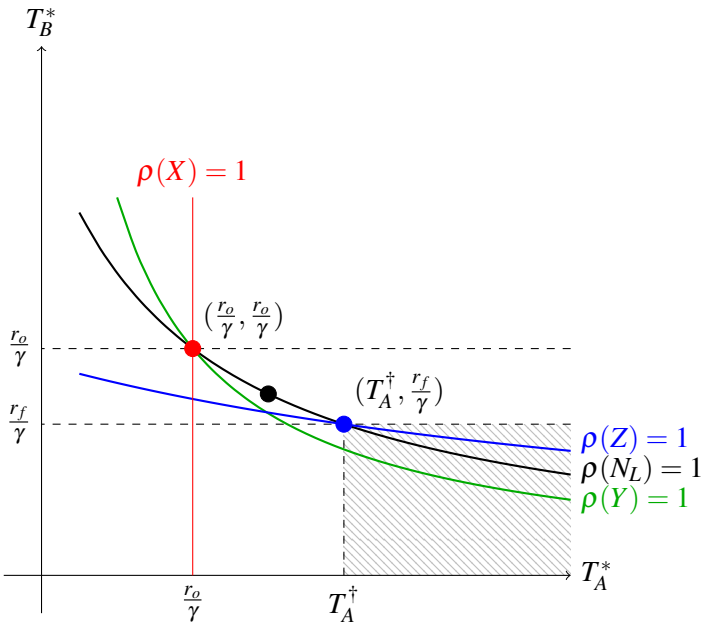

Supplementary Figure 5: Invasion boundaries and ESCs for Scenario 5. The red line shows the invasion boundary of non-sinking life cycles $X+1$. The green line represents the invasion boundary of a sinking life cycle that avoids oxygen deprivation ($Y+1$ with $Y < N_L$). The black line corresponds to the largest such life cycle, N_L+1. The blue line represents the invasion boundary of a sinking life cycles that experiences oxygen deprivation ($Z+1$ with $Z > N_L$). Points indicate ESCs: coexistence of all life cycles up to N_L+1 (red; regime V from the main text); dominance of N_L+1 (black; regime III from the main text); and coexistence of N_L+1 with all larger life cycles (blue; regime V from Extended Data Figure 4). Sufficiently large life cycles cannot exist in isolation in the shaded region because of Result S4.7.

- dominance of the largest sinking life cycle that avoids oxygen deprivation (N_L+1) (Supplementary Figure 5, black point; regime III in the main text);
- coexistence of N_L+1 and all sinking life cycles that experience oxygen deprivation at the blue point (Fig. 5, blue point; regime V in the Extended Data Figure 4).

We have now exhausted all scenarios, completing the proof of Result S4.8.

S4.4 Evolutionary dynamics leading to broad coexistence

In this subsection, we analyze the evolutionary dynamics that give rise to broad coexistence. For simplicity, we focus on the anoxic regime, in which $N_U = N_L = 0$ (or, equivalently, $r_o = r_f$), but analogous results can be obtained for other scenarios where there are no differences in growth rates within each layer. In the anoxic regime, all cells divide at rate r_f. The invasion boundary for non-sinking life cycles is now the vertical line $T_A^* = \frac{r_f}{\gamma}$. Moreover, as we saw in Subsection S4.3, the ESC consists of all life cycles and corresponds to the *broad coexistence point* $(T_A^*, T_B^*) = (\frac{r_f}{\gamma}, \frac{r_f}{\gamma})$. In this subsection, we show how this ESC is reached.

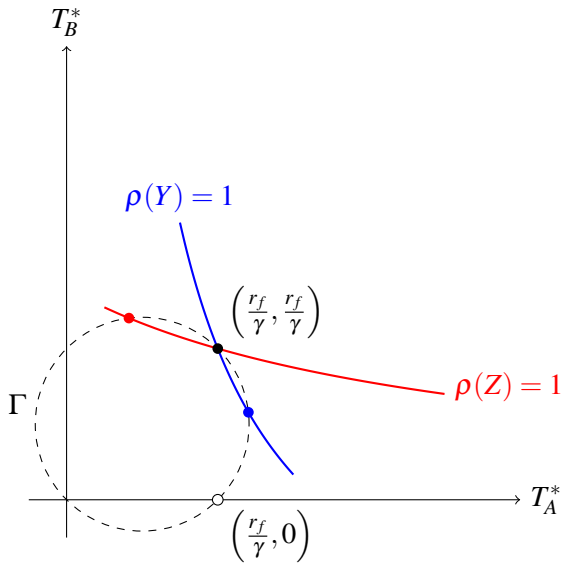

Supplementary Figure 6: In isolation, a sinking life cycle reaches steady state at the second intersection point of the circle Γ and the line $\rho = 1$ (i.e., the intersection point other than $(\frac{r_f}{\gamma}, \frac{r_f}{\gamma})$). So the blue point corresponds to the steady state of $Y+1$ in isolation and the red point corresponds to the steady state of $Z+1$ in isolation.

In the anoxic regime, the change in the total density of cells $T = T_A + T_B$ is given by

$$\frac{dT}{dt} = r_f T_A + r_f T_B - \gamma(T_A^2 + T_B^2). \tag{115}$$

At steady state, we must therefore always have $r_f(T_A^* + T_B^*) = \gamma((T_A^*)^2 + (T_B^*)^2)$. In (T_A^*, T_B^*)-space, this equation describes a circle Γ that passes through the origin, the point $(\frac{r_f}{\gamma}, 0)$ where all non-sinking life cycles that avoid oxygen deprivation can neutrally coexist, and the broad coexistence point $(\frac{r_f}{\gamma}, \frac{r_f}{\gamma})$ (see Supplementary Figure 6).

Steady states of sinking life cycles in isolation

The steady state of a sinking life cycle $Y+1$ in isolation must lie on the circle Γ and on the invasion boundary $\rho(Y) = 1$. These two curves intersect at $(\frac{r_f}{\gamma}, \frac{r_f}{\gamma})$. Because of the shape of the invasion boundary (Result S4.3), the invasion boundary and Γ intersect again at one other point (Supplementary Figure 6). We claim that this second intersection point corresponds to the steady state of the life cycle in isolation.

Result S4.10: Steady state of a sinking life cycle in isolation

In the anoxic regime, the steady state of a sinking life cycle in isolation corresponds to the second intersection point (i.e., the intersection point other than $(\frac{r_f}{\gamma}, \frac{r_f}{\gamma})$) of the invasion boundary and Γ.

To establish Result S4.10, we have to show that the life cycle cannot exist in isolation at $(T_A^*, T_B^*) = (\frac{r_f}{\gamma}, \frac{r_f}{\gamma})$. To do this, we note that the population dynamics of a sinking life cycle $N+1$ are given by

$$\begin{cases} \dot{x_1} = -r_f x_1 - \gamma T_A x_1 + N r_f x_N, \\ \dot{x_i} = r_f(i-1)x_{i-1} - r_f i x_i - \gamma T_A x_i, & \text{for} \quad 1 < i < N_S, \\ \dot{x_i} = r_f(i-1)x_{i-1} - r_f i x_i - \gamma T_B x_i, & \text{for} \quad N_S \leq i < N, \\ \dot{x_N} = r_f(N_1)x_{N-1} - \gamma T_B x_N. \end{cases} \tag{116}$$

If the life cycle is at steady state *and* we also have $T_A^* = T_B^* = \frac{r_f}{\gamma}$, we therefore must have

$$0 = \dot{x_1} = -r_f x_1 - r_f x_1 + N r_f x_N = r_f(-2x_1 + N x_N), \tag{117}$$

$$0 = \dot{x_i} = r_f(i-1)x_{i-1} - r_f i x_i - r_f x_i = r_f((i-1)x_{i-1} - (i+1)x_i), \qquad \text{for} \quad 1 < i < N, \tag{118}$$

$$0 = \dot{x_N} = r_f(N_1)x_{N-1} - r_f x_N = r_f((N-1)x_{N-1} - x_N). \tag{119}$$

For $1 < i < N$ we see that $(i+1)x_i = (i-1)x_{i-1}$, which leads to

$$x_i = \frac{i-1}{i+1} \cdot x_{i-1} = \frac{i-1}{i+1} \cdot \frac{i-2}{i} \cdot x_{i-2} = \cdots = \frac{(i-1)!}{(i+1)!/2} \cdot x_1 = \frac{2}{i(i+1)} \cdot x_1. \tag{120}$$

Moreover, (117) tells us that $x_N = \frac{2}{N} \cdot x_1$. We conclude that if the life cycle $N+1$ exists at steady state with $T_A^* = T_B^* = \frac{r_f}{\gamma}$, then

$$(x_1, x_2, \ldots, x_N) = x_1 \cdot \left(\frac{2}{1\cdot 2}, \frac{2}{2\cdot 3}, \frac{2}{3\cdot 4}, \frac{2}{4\cdot 5}, \ldots, \frac{2}{N\cdot(N+1)}, \frac{2}{N} \right). \tag{121}$$

However, when the life cycle is in isolation, the population structure (121) is not compatible with $T_A^* = T_B^*$. Indeed, it would lead to

$$\frac{T_A^*}{T_A^* + T_B^*} = \frac{\sum_{i=1}^{N_S - 1} i x_i}{\sum_{i=1}^{N} i x_i} = \frac{\frac{1}{2} + \frac{1}{3} + \ldots + \frac{1}{N_S}}{\frac{1}{2} + \frac{1}{3} + \ldots + \frac{1}{N} + 1},$$

of which we can show[1] that it is not equal to $\frac{1}{2}$ unless $N = 1$ and $N_S = 2$, which would contradict $N_S \leq N$. We conclude that the life cycle $N+1$ cannot exist in isolation at a steady state with $T_A^* = T_B^* = \frac{r_f}{\gamma}$. Therefore, the $N+1$-only steady state must correspond to the second intersection of the invasion boundary and Γ.

Intermediate and large life cycles

The intersection of the invasion boundary and Γ corresponding to a sinking life cycle in isolation can lie on either side of the line $T_A^* = \frac{r_f}{\gamma}$. For example, in Supplementary Figure 6, the steady state of $Y+1$ in isolation

[1] In fact, $(N_S, N) = (2, 1)$ is the only solution to the equation $2(H_{N_S} - 1) = H_N$, where $H_n = \frac{1}{1} + \frac{1}{2} + \ldots + \frac{1}{n}$ denotes the n-th harmonic number. We sketch a quick proof of this fact. First, check by hand that there are no other solutions with $N \leq 81$. Then, if $N \geq 82$, we use the inequalities $\log(n) \leq H_n \leq \log(n) + 1$ to deduce that

$$2(\log N_S - 1) \leq 2(H_{N_S} - 1) = H_N \leq \log N + 1,$$

which implies $N_S^2 \leq e^3 N \leq \frac{N^2}{4}$ (here we use $N \geq 82$) and therefore $N_S \leq \frac{N}{2}$. By the Bertrand-Chebyshev theorem, there is a prime $\frac{N}{2} < p < N$. However, now p occurs in the denominator of H_N (when simplified as fraction) but not in that of $2(H_{N_S} - 1)$, so $2(H_{N_S} - 1)$ and H_N cannot be equal to each other.

(the red point) satisfies $T_A^* > \frac{r_f}{\gamma}$, while the steady state of $Z+1$ in isolation (the blue point) satisfies $T_A^* < \frac{r_f}{\gamma}$. In light of Result S4.5, all sufficiently large life cycles will intersect Γ to the left of the line $T_A^* = \frac{r_f}{\gamma}$ (we will call such life cycles simply *large*), whereas all sufficiently small sinking life cycles will intersect Γ to the right of the line $T_A^* = \frac{r_f}{\gamma}$ (we will call such life cycles *intermediate*). Equivalently, intermediate life cycles satisfy $T_A^* > T_B^*$ and have the majority of their cell population in the upper layer (when in isolation and at steady state) , whereas large life cycles satisfy $T_A^* < T_B^*$ and have the majority of their cell population in the lower layer (when in isolation and at steady state).

The following result addresses the threshold at which life cycles become large.

Result S4.11: Large life cycles

In the anoxic regime, a sinking life cycle is large if

$$1+\frac{1}{N_S+1}+\frac{1}{N_S+2}+\ldots+\frac{1}{N} > \frac{1}{2}+\frac{1}{3}+\ldots+\frac{1}{N_S} \tag{122}$$

and intermediate otherwise.

To establish Result S4.11, we see from Supplementary Figure 6 that a life cycle will be large when the slope of the life cycle's invasion boundary at $(T_A^*, T_B^*) = (\frac{r_f}{\gamma}, \frac{r_f}{\gamma})$ is larger than $\left.\frac{d\Gamma}{dT_A^*}\right|_{T_A^*=r_f/\gamma} = -1$ and intermediate otherwise. According to (92), the derivative of the invasion boundary at $(T_A^*, T_B^*) = (\frac{r_f}{\gamma}, \frac{r_f}{\gamma})$ is equal to

$$\frac{dT_B^*}{dT_A^*} = -\frac{\sum_{1\le i<N_S} \frac{\gamma}{ir_f+\gamma\cdot\frac{r_f}{\gamma}}}{\frac{\gamma}{r_f}+\sum_{N_S\le i<N} \frac{\gamma}{ir_f+\gamma\cdot\frac{r_f}{\gamma}}} = -\frac{\frac{1}{2}+\frac{1}{3}+\ldots+\frac{1}{N_S}}{1+\frac{1}{N_S+1}+\frac{1}{N_S+2}+\ldots+\frac{1}{N}}, \tag{123}$$

and Result S4.11 follows.

Note that Result S4.11 implies that large life cycles always exist, because the harmonic series diverges (the same conclusion also follows from Result S4.7). Moreover, Result S4.11 provides a straightforward way to calculate at what size life cycles become large. For example, for $N_S = 20$, we find using Result S4.11 that the smallest large life cycle N^*+1 has $N^* = 101$, which is exactly what we observe in our simulations.

Evolutionary dynamics for the anoxic regime

The invasion rules for the anoxic regime are as follows:

Result S4.12: Invasion rules for the anoxic regime

In the anoxic regime:

(i) Non-sinking life cycles can be invaded by any sinking life cycle;

(ii) An intermediate life cycle in isolation can be invaded by any larger intermediate life cycle and by any large life cycle, but not by any other life cycle;

(iii) A large life cycle in isolation can be invaded by any smaller life cycle, irrespective of whether it is non-sinking, intermediate, or large.

All these properties follow from careful consideration of the invasion boundaries and the locations of the steady states (see Supplementary Figure 7 for an example). For (i), we simply note that the steady state of non-sinking life cycles exists at $(T_A^*, T_B^*) = (\frac{r_f}{\gamma}, 0)$, which lies below the invasion boundary of all sinking life cycles. For (ii), we note that the steady state of an intermediate life cycle corresponds to a point (T_A^*, T_B^*) where $T_A^* > \frac{r_f}{\gamma}$ and $T_B^* < \frac{r_f}{\gamma}$; therefore, non-sinking life cycles cannot invade. But the point $(T_A^*, T_B)^*$ lies below the invasion boundaries of all larger life cycles, which therefore are able to invade. Finally, for (iii), the steady state (T_A^*, T_B^*) now satisfies $T_A^* < \frac{r_f}{\gamma}$ but $T_B^* > \frac{r_f}{\gamma}$. We now see that all smaller life cycles can invade, including the non-sinking life cycles.

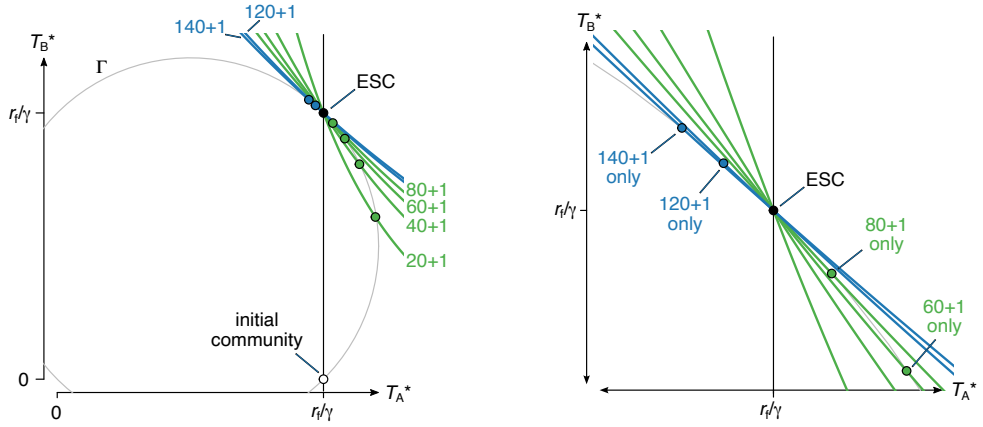

Supplementary Figure 7: Invasion boundaries and communities for the anoxic regime. The colored lines indicate the invasion boundaries of non-sinking life cycles (black), intermediate life cycles (green), and large life cycles (blue). The colored points correspond to possible steady-state communities with only non-sinking life cycles present (white), a sinking life cycle in isolation (green or blue), or the broad coexistence point (black). The broad coexistence point is the ESC: it is the only steady state community that cannot be invaded by any life cycle. The diagram on the right is a closeup of the diagram on the left. In this example, $N_S = 20$.

Result S4.12 explains the dynamics observed for the broad coexistence regime in the simulations. Starting from the unicellular ancestor, sinking life cycles can invade (i). If an intermediate life cycle invades, the unicellular ancestor (and any other sinking life cycles) are displaced (ii), and selection favors increasing

size: intermediate life cycles larger than the resident can successively invade and displace it. This selection for increasing size continues until a large life cycle invades. Then, coexistence instead of displacement results (iii). This coexistence leads to $T_A^* = T_B^* = \frac{r_f}{\gamma}$; after all, the invasion boundaries of two sinking life cycles intersect only at the point $(T_A^*, T_B^*) = (\frac{r_f}{\gamma}, \frac{r_f}{\gamma})$. Once this happens, broad coexistence is established: the point $(T_A^*, T_B^*) = (\frac{r_f}{\gamma}, \frac{r_f}{\gamma})$ in fact lies on *all* the invasion boundaries, and so all the life cycles can invade neutrally. The same ESC is reached when a large life cycle invades the unicellular ancestor instead of an intermediate one; in that case, we immediately reach broad coexistence.

S4.5 Condition for invasion of sinking life cycles with mixing

Here, we explore whether the unicellular ancestor can be invaded by a sinking life cycle when there is mixing. In the case of perfect spatial separation ($q_B = 0$), we have $T_B^* = 0$ when only the unicellular ancestor is present, leading to $\rho(n) \to \infty$ for any $n \geq N_S$ (see equation (87)). Therefore, in the absence of mixing, the unicellular ancestor can be invaded by any sinking life cycle. This is not necessarily true when we allow for mixing. However, under some conditions we can show that the ancestor will still be invaded by sufficiently large sinking life cycles.

Result S4.13: Invasion of sinking life cycle with mixing

If the unicellular ancestor's steady state satisfies $T_B^* < \frac{r_f}{\gamma}$, then it can be invaded by a sufficiently large sinking life cycle.

Recall that for sinking life cycles that experience oxygen deprivation ($N > N_L$), we have the recurrence relation

$$\frac{\rho(N+1)}{\rho(N)} = \frac{N\bar{r}_N + r_f}{N\bar{r}_N + \gamma T_B^*} \tag{124}$$

(see (94)). Therefore, when $T_B^* < \frac{r_f}{\gamma}$, the reproduction numbers $\rho(N)$ are increasing for large enough N. We will now establish the stronger statement that, in fact, we must have $\rho(N) > 1$ for large enough N. From (124) we obtain

$$\rho(N) = \rho(N_L) \prod_{i=N_L}^{N-1} \frac{i\bar{r}_i + r_f}{i\bar{r}_i + \gamma T_B^*} \tag{125}$$

for $N > N_L$, or, taking logarithms,

$$\log(\rho(N)) = \log(\rho(N_L)) + \sum_{i=N_L}^{N-1} \log\left(\frac{i\bar{r}_i + r_f}{i\bar{r}_i + \gamma T_B^*}\right) = \log(\rho(N_L)) + \sum_{i=N_L}^{N-1} \log\left(\frac{\Lambda + i + 1}{\Lambda + i + \eta}\right), \tag{126}$$

where $\eta = \gamma T_B^*/r_f < 1$ and $\Lambda = \left(\frac{r_o}{r_f} - 1\right) N_L$. Because $\eta < 1$ and $\Lambda > 0$, each summand is positive. Moreover, for large i we know that

$$\log\left(\frac{\Lambda + i + 1}{\Lambda + i + \eta}\right) = \log\left(1 + \frac{1 - \eta}{\Lambda + i + \eta}\right) \geq \frac{1}{2} \cdot \frac{1 - \eta}{\Lambda + i + \eta}, \tag{127}$$

where the inequality holds for all sufficiently large i because $\log(1+x) \geq x/2$ for small $x > 0$. Hence, for sufficiently large N, we have

$$\log \rho(N) \geq C + \frac{1-\eta}{2} \sum_{i=N_{\text{large}}}^{N-1} \frac{1}{\Lambda + i + \eta}, \tag{128}$$

where N_{large} is chosen large enough to satisfy (127) and C is a constant absorbing the finite sum

$$\sum_{i=N_S}^{N_{\text{large}}-1} \log\big((\Lambda+i+1)/(\Lambda+i+\eta)\big). \tag{129}$$

Because the harmonic series diverges, so does the sum on the right in (128), and therefore $\rho(N) \to \infty$ as $N \to \infty$. In particular, for sufficiently large N, we have $\rho(N) > 1$. This establishes Result S4.13.

The condition of Result S4.13 will be satisfied provided that there is not too much mixing.

Result S4.14: The unicellular ancestor can be invaded for low enough mixing

If $N_U > 0$, then the unicellular ancestor can be invaded by a sufficiently large sinking life cycle if $N_L > 0$ and $\dfrac{q_B}{q_B^2 + (1-q_B)^2} < \dfrac{r_f}{r_o}$, and also if $N_L = 0$ and $\dfrac{q_B}{1-q_B} < \dfrac{r_f}{r_o}$.

When we allow for mixing, the unicellular ancestor's dynamics are given by

$$\frac{dy}{dt} = r_o q_A y + r_B q_B y - \gamma(q_A^2 + q_B^2) y^2, \tag{130}$$

where r_o is the reproduction rate of single cells in the upper layer (after all, we assume $N_L > 0$), and r_B is the reproduction rate of single cells in the lower layer, which can be either r_o or r_f depending on whether $N_L > 0$ or $N_L = 0$. The unicellular ancestor's steady state therefore is

$$y^* = \frac{r_o q_A + r_B q_B}{\gamma(q_A^2 + q_B^2)}. \tag{131}$$

At this equilibrium, we find

$$T_B^* = q_B y^* = \frac{q_B(r_o q_A + r_B q_B)}{\gamma(q_A^2 + q_B^2)}. \tag{132}$$

When $N_L > 0$, we have $r_B = r_o$. In this case, we have

$$T_B^* < \frac{r_f}{\gamma} \iff \frac{q_B r_o}{\gamma(q_A^2 + q_B^2)} < \frac{r_f}{\gamma} \iff \frac{q_B}{q_A^2 + q_B^2} < \frac{r_f}{r_o}. \tag{133}$$

On the other hand, when $N_L = 0$, we have $r_B = r_f$, and so

$$T_B^* < \frac{r_f}{\gamma} \iff \frac{q_B(q_A r_o + q_B r_f)}{\gamma(q_A^2 + q_B^2)} < \frac{r_f}{\gamma} \iff \frac{q_B}{q_A} < \frac{r_f}{r_o}. \tag{134}$$

This establishes Result S4.14.

For the parameter values in the main text ($r_o = 6.8$, $r_f = 1.0$), the inequality $\frac{q_B}{q_B^2+(1-q_B)^2} < \frac{r_f}{r_o}$ from Result S4.14 is satisfied for $q_B < 0.117$, whereas the inequality $\frac{q_B}{1-q_B} < \frac{r_f}{r_o}$ is satisfied for $q_B < 0.128$.

A Appendix: mathematical analysis for the $N \times 1$ and $N/2+N/2$ life cycles

A.1 Life cycle $N \times 1$

In this life cycle, once groups reach N cells, they instantaneously disintegrate into N single-cell propagules. The density of groups in environments A and B of a $N \times 1$ life cycle changes according to

$$\frac{dx_{1,A}}{dt} = N(N-1)r_{N-1,A}x_{N-1,A} - r_{1,A}x_{1,A} - \gamma T_A(y,\vec{x})x_{1,A} - m_{1,AB}x_{1,A} + m_{1,BA}x_{1,B}, \tag{135}$$

$$\frac{dx_{1,B}}{dt} = N(N-1)r_{N-1,A}x_{N-1,A} - r_{1,B}x_{1,B} - \gamma T_B(y,\vec{x})x_{1,B} - m_{1,BA}x_{1,B} + m_{1,AB}x_{1,A} \tag{136}$$

for single cells, and

$$\frac{dx_{i,A}}{dt} = (i-1)r_{i-1,A}x_{i-1,A} - ir_{i,A}x_{i,A} - \gamma T_A(y,\vec{x})x_{i,A} - m_{i,AB}x_{i,A} + m_{i,BA}x_{i,B}, \tag{137}$$

$$\frac{dx_{i,B}}{dt} = (i-1)r_{i-1,B}x_{i-1,B} - ir_{i,B}x_{i,B} - \gamma T_B(y,\vec{x})x_{i,B} - m_{i,BA}x_{i,B} + m_{i,AB}x_{i,A} \tag{138}$$

for groups of size $1 < n \leq N$.

A.1.1 Invasion of a mutant of the $N \times 1$ life cycle

Following the same analysis from section S2.3, we find the reproduction number of a $N \times 1$ life cycle:

$$\rho(N) = N \prod_{n=1}^{N-1} \frac{n\bar{r}_n}{n\bar{r}_n + \bar{c}_n^*} \tag{139}$$

$$= N! \prod_{n=1}^{N-1} \frac{1}{n + \frac{C_n}{R_n}}. \tag{140}$$

Thus, if

$$N! \prod_{n=1}^{N-1} \frac{1}{n + \frac{C_n}{R_n}} > 1, \tag{141}$$

a multicellular mutant of the $N \times 1$ life cycle invades the unicellular ancestor population.

A.1.2 Extension for fast migration and multiple $N \times 1$ life cycles

Here, differently from the $N+1$ case, we have $y = x_1^2$, since a unicellular life cycle corresponds to 2×1. Following section S3.1, the dynamics of a community of $N \times 1$ life cycles under the fast migration limit is

$$\frac{dx_1^2}{dt} = (\bar{r}_1 - \bar{c}_1(\vec{x}))x_1^2, \tag{142}$$

for $N=1$, and

$$\frac{dx_1^N}{dt} = N(N-1)\bar{r}_{N-1}x_{N-1}^N - (\bar{r}_1 + \bar{c}_1(\vec{x}))\,x_1^N, \tag{143}$$

$$\frac{dx_i^N}{dt} = (i-1)\bar{r}_{i-1}x_{i-1}^N - (i\bar{r}_i + \bar{c}_i(\vec{x}))\,x_i^N \tag{144}$$

for $1 < i < N$ and $1 < N$. As in the $N+1$ model, $T_A(\vec{x}) \coloneqq \sum_N \sum_n n p_{n,A} x_n^N$ and $T_B(\vec{x}) \coloneqq \sum_N \sum_n n p_{n,B} x_n^N$. The average death rate—from competition—of cells in a group of size n is $\bar{c}_n(\vec{x}) = \gamma(p_{n,A}T_A(\vec{x}) + p_{n,B}T_B(\vec{x}))$ and the average growth rate of cells in a group of size n is $\bar{r}_n = p_{n,A}r_{n,A} + p_{n,B}r_{n,B}$. The basic reproduction number is the same as in (139), but with the updated expressions of $\bar{r}_i$ and $\bar{c}_i$ above.

A.2 Life cycle $N/2+N/2$

In this life cycle, once groups reach N cells, they instantaneously split into two groups of equal size. If N is odd, one of the fragments ends up with an extra cell (i.e., one group with $\frac{N+1}{2}$ cells and another with $\frac{N-1}{2}$ cells). For an even value of N, the density of groups in environment A and B of a $N/2+N/2$ life cycle changes according to

$$\frac{dx_{N/2,A}}{dt} = 2(N-1)r_{N-1,A}x_{N-1,A} - \frac{N}{2}r_{N/2,A}x_{N/2,A} - \gamma T_A(y,\vec{x})x_{N/2,A} - m_{N/2,AB}x_{N/2,A} + m_{N/2,BA}x_{N/2,B}, \tag{145}$$

$$\frac{dx_{N/2,B}}{dt} = 2(N-1)r_{N-1,A}x_{N-1,A} - \frac{N}{2}r_{N/2,B}x_{N/2,B} - \gamma T_B(y,\vec{x})x_{N/2,B} - m_{N/2,BA}x_{N/2,B} + m_{N/2,AB}x_{N/2,A} \tag{146}$$

for the smallest size of the life cycle ($N/2$), and

$$\frac{dx_{i,A}}{dt} = (i-1)r_{i-1,A}x_{i-1,A} - r_{i,A}x_{i,A} - \gamma T_A(y,\vec{x})x_{i,A} - m_{i,AB}x_{n,A} + m_{i,BA}x_{i,B}, \tag{147}$$

$$\frac{dx_{i,B}}{dt} = (i-1)r_{i-1,B}x_{i-1,B} - r_{i,B}x_{i,B} - \gamma T_B(y,\vec{x})x_{i,B} - m_{i,BA}x_{i,B} + m_{i,AB}x_{i,A}. \tag{148}$$

for $N/2 < i < N$. When N is odd,

$$\frac{dx_{\frac{N-1}{2},A}}{dt} = (N-1)r_{N-1,A}x_{N-1,A} - \frac{N-1}{2}r_{\frac{N-1}{2},A}x_{\frac{N-1}{2},A} - \gamma T_A(y,\vec{x})x_{\frac{N-1}{2},A} - m_{\frac{N-1}{2},AB}x_{\frac{N-1}{2},A} + \tag{149}$$

$$+ m_{\frac{N-1}{2},BA}x_{\frac{N-1}{2},B}, \tag{150}$$

$$\frac{dx_{\frac{N-1}{2},B}}{dt} = (N-1)r_{N-1,B}x_{N-1,B} - \frac{N-1}{2}r_{\frac{N-1}{2},B}x_{\frac{N-1}{2},B} - \gamma T_B(y,\vec{x})x_{\frac{N-1}{2},B} - m_{\frac{N-1}{2},BA}x_{\frac{N-1}{2},B} + \tag{151}$$

$$+ m_{\frac{N-1}{2},AB}x_{\frac{N-1}{2},A}, \tag{152}$$

$$\frac{dx_{\frac{N+1}{2},A}}{dt} = (N-1)r_{N-1,A}x_{\frac{N-1}{2},A} + \frac{N-1}{2}r_{\frac{N-1}{2},A}x_{N-1,A} - \frac{N+1}{2}r_{\frac{N+1}{2},A}x_{\frac{N+1}{2},A} - \gamma T_A(y,\vec{x})x_{\frac{N+1}{2},A} - \tag{153}$$

$$- m_{\frac{N+1}{2},AB}x_{\frac{N+1}{2},A} + m_{\frac{N+1}{2},BA}x_{\frac{N+1}{2},B}, \tag{154}$$

$$\frac{dx_{\frac{N+1}{2},B}}{dt} = (N-1)r_{N-1,B}x_{N-1,B} + \frac{N-1}{2}r_{\frac{N-1}{2},B}x_{\frac{N-1}{2},B} - \frac{N+1}{2}r_{\frac{N+1}{2},B}x_{\frac{N+1}{2},B} - \gamma T_B(y,\vec{x})x_{\frac{N+1}{2},B} - \tag{155}$$

$$- m_{\frac{N+1}{2},BA}x_{\frac{N+1}{2},B} + m_{\frac{N+1}{2},AB}x_{\frac{N+1}{2},A} \tag{156}$$

for the smallest sizes of the life cycle ($\frac{N-1}{2}$ and $\frac{N+1}{2}$), and

$$\frac{dx_{i,A}}{dt} = (i-1)r_{i-1,A}x_{i-1,A} - ir_{i,A}x_{i,A} - \gamma T_A(y,\vec{x})x_{i,A} - m_{i,AB}x_{n,A} + m_{i,BA}x_{i,B}, \tag{157}$$

$$\frac{dx_{i,B}}{dt} = (i-1)r_{i-1,B}x_{i-1,B} - ir_{i,B}x_{i,B} - \gamma T_B(y,\vec{x})x_{i,B} - m_{i,BA}x_{i,B} + m_{i,AB}x_{i,A}. \tag{158}$$

for $N/2 < i < N$. Notice that groups smaller than $N/2$ (or $\frac{N-1}{2}$ when N is odd) cannot exist as the smallest propagules produced after fragmentation are of size $N/2$ and groups cannot lose cells otherwise.

A.2.1 Invasion of a multicellular mutant of the $N/2+N/2$ life cycle

Following the same analysis from section S2.3, we find the reproduction number of a $N/2+N/2$ life cycle:

$$\rho(N) = \begin{cases} 2\prod_{n=N/2}^{N-1} \frac{n\bar{r}_n}{n\bar{r}_n + \bar{c}_n^*}, & \text{for } N \text{ even} \\ \left(1 + \frac{\frac{N-1}{2}\bar{r}_{(N-1)/2}}{\frac{N-1}{2}\bar{r}_{(N-1)/2} + \bar{c}^*_{(N-1)/2}}\right) \prod_{n=(N+1)/2}^{N-1} \frac{n\bar{r}_n}{n\bar{r}_n + \bar{c}_n^*}, & \text{for } N \text{ odd} \end{cases} \tag{159}$$

or

$$\rho(N) = \begin{cases} 2\frac{(N-1)!}{(\frac{N-1}{2})!}\prod_{n=N/2}^{N-1} \frac{1}{n + \frac{C_n}{R_n}}, & \text{for } N \text{ even} \\ \frac{(N-1)!}{(\frac{N+1}{2})!}\left(1 + \frac{\frac{N-1}{2}}{\frac{N-1}{2} + \frac{C_{(N-1)/2}}{R_{(N-1)/2}}}\right) \prod_{n=(N+1)/2}^{N-1} \frac{1}{n + \frac{C_n}{R_n}}. & \text{for } N \text{ odd} \end{cases} \tag{160}$$

Thus, if $\rho(N) > 1$, a multicellular mutant of the $N/2+N/2$ life cycle invades.

A.2.2 Extension for fast migration and multiple $N/2+N/2$ life cycles

Here, differently from the $N+1$ case, we have $y = x_1^2$, since a unicellular life cycle corresponds to $2/2+2/2$. Following section S3.1, the dynamics of a community of $N/2+N/2$ life cycles under the fast migration limit is

$$\frac{dx_1^2}{dt} = (\bar{r}_1 - \bar{c}_1(\vec{x}))x_1^2, \tag{161}$$

for $N = 1$,

$$\frac{dx_{N/2}^N}{dt} = 2(N-1)\bar{r}_N x_{N-1}^N - \left(\frac{N}{2}\bar{r}_{N/2} + \bar{c}_{N/2}(\vec{x})\right)x_{N/2}^N, \tag{162}$$

$$\frac{dx_i^N}{dt} = (i-1)\bar{r}_{i-1}x_{i-1}^N - (i\bar{r}_i + \bar{c}_i(\vec{x}))x_i^N, \tag{163}$$

for N even and $N/2 < i < N$, and

$$\frac{dx^N_{\frac{N-1}{2}}}{dt} = (N-1)\bar{r}_N x^N_{N-1} - \left(\frac{N-1}{2}\bar{r}_{\frac{N-1}{2}} + \bar{c}_{\frac{N-1}{2}}(\vec{x})\right) x^N_{\frac{N-1}{2}}, \tag{164}$$

$$\frac{dx^N_{\frac{N+1}{2}}}{dt} = (N-1)\bar{r}_N x^N_{N-1} + \frac{N-1}{2}\bar{r}_{\frac{N-1}{2}} x^N_{\frac{N-1}{2}} - \left(\frac{N+1}{2}\bar{r}_{\frac{N+1}{2}} + \bar{c}_{\frac{N+1}{2}}(\vec{x})\right) x^N_{\frac{N+1}{2}}, \tag{165}$$

$$\frac{dx^N_i}{dt} = (i-1)\bar{r}_{i-1} x^N_{i-1} - (i\bar{r}_i + \bar{c}_i(\vec{x})) x^N_i, \tag{166}$$

for N odd and $\frac{N+1}{2} < i < N$. As in the $N+1$ model, $T_A(\vec{x}) \coloneqq \sum_N \sum_n n p_{n,A} x^N_n$ and $T_B(\vec{x}) \coloneqq \sum_N \sum_n n p_{n,B} x^N_n$. The average death rate—from competition—of cells in a group of size n is $\bar{c}_n(\vec{x}) = \gamma(p_{n,A} T_A(\vec{x}) + p_{n,B} T_B(\vec{x}))$ and the average growth rate of cells in a group of size n is $\bar{r}_n = p_{n,A} r_{n,A} + p_{n,B} r_{n,B}$. The basic reproduction number is the same as in (139), but with the updated expressions of $\bar{r}_i$ and $\bar{c}_i$ above.

Data Accessibility

All the scripts needed to replicate the results presented here are available at [1].

References

[1] D. Jorge. Code for: Direct benefits are not necessary for the evolution of multicellularity, 2025. https://doi.org/10.5281/zenodo.18749114.

[2] V. Ress, A. Traulsen, and Y. Pichugin. Eco-evolutionary dynamics of clonal multicellular life cycles. *Elife*, 11:e78822, 2022.